Climate Dynamics (2005) 25: 75–98
DOI 10.1007/s00382-005-0016-5

**Ramzi Touchan · Elena Xoplaki · Gary Funkhouser
Jürg Luterbacher · Malcolm K. Hughes · Nesat Erkan
Ünal Akkemik · Jean Stephan**

Reconstructions of spring/summer precipitation for the Eastern Mediterranean from tree-ring widths and its connection to large-scale atmospheric circulation

Received: 30 August 2004 / Accepted: 14 February 2005

Abstract This study represents the first large-scale systematic dendroclimatic sampling focused on developing chronologies from different species in the eastern Mediterranean region. Six reconstructions were developed from chronologies ranging in length from 115 years to 600 years. The first reconstruction (1885–2000) was derived from principal components (PCs) of 36 combined chronologies. The remaining five, 1800–2000, 1700–2000, 1600–2000, 1500–2000 and 1400–2000 were developed from PCs of 32, 18, 14, 9, and 7 chronologies, respectively. Calibration and verification statistics for the period 1931–2000 show good levels of skill for all reconstructions. The longest period of consecutive dry years, defined as those with less than 90% of the mean of the observed May–August precipitation, was 5 years (1591–1595) and occurred only once during the last 600 years. The longest reconstructed wet period was 5 years (1601–1605 and 1751–1755). No long term trends were found in May–August precipitation during the last few centuries. Regression maps are used to identify the influence of large-scale atmospheric circulation on regional precipitation. In general, tree-ring indices are influenced by May–August precipitation, which is driven by anomalous below (above) normal pressure at all atmospheric levels and by convection (subsidence) and small pressure gradients at sea level. These atmospheric conditions also control the anomaly surface air temperature distribution which indicates below (above) normal values in the southern regions and warmer (cooler) conditions north of around 40°N. A compositing technique is used to extract information on large-scale climate signals from extreme wet and dry summers for the second half of the twentieth century and an independent reconstruction over the last 237 years. Similar main modes of atmospheric patterns and surface air temperature distribution related to extreme dry and wet summers were identified both for the most recent 50 years and the last 237 years. Except for the last few decades, running correlation analyses between the major European-scale circulation patterns and eastern Mediteranean spring/summer precipitation over the last 237 years are non-stationary and insignificant, suggesting that local and/or sub-regional geographic factors and processes are important influences on tree-ring variability over the last few centuries.

R. Touchan (✉) · G. Funkhouser · M. K. Hughes
Laboratory of Tree-Ring Research, The University of Arizona, P.O. Box 210058, Tucson, AZ, 85721-0058 USA
E-mail: rtouchan@ltrr.arizona.edu
Tel.: +1-520-6212992
Fax: +1-520-6218229

E. Xoplaki · J. Luterbacher
Institute of Geography and NCCR Climate, University of Bern, Hallerstrasse 12, 3012 Bern, Switzerland

N. Erkan
Southwest Anatolia Forest research Institute (SAFRI), POB 264, Antalya, Turkey

Ünal Akkemik
Faculty of Forestry, Department of Forest Botany, University of Istanbul, 34473 Bahçeköy-Istanbul, Turkey

J. Stephan
Forestry Department, Ministry of Agriculture, Beirut, Lebanon

1 Introduction

The Mediterranean region is climate-sensitive, stressed by extremes of heat, highly variable precipitation, and limited water resources. These features are of great significance to the growing human populations of the area. High (monthly, seasonal, annual and interannual) and low (interdecadal to century) frequency variations of precipitation play a crucial role in the regional agriculture, ecosystems, environment and socio-economics and water resources (Türkeş 1998; Mann 2002; Xoplaki et al. 2000, 2004). Regional climate variability results from the interactions of local factors and a variety of large-scale

circulation features. Some of the main physical and physico-geographical factors controlling the spatial distribution of climatic conditions over the Mediterranean include atmospheric circulation, latitude, altitude (orography), Atlantic and Mediterranean sea surface temperatures, land-sea interactions (distance from the sea), and smaller-scale processes (Lolis et al. 1999; Xoplaki et al. 2000, 2003a, b, 2004).

Natural and human systems are vulnerable to the scarcity and irregular availability of water resources that characterize the region's climate. This is due mainly to the high seasonal and year-to-year variability of precipitation. In the Mediterranean region, where most of the annual rainfall occurs during the winter half-year, severe water deficits can occur during the growing season even when there is sufficient annual precipitation. This is especially true in the eastern Mediterranean and Near East (e.g. Tarawneh and Kadioglu 2003).

These climatic features can play a role in the dynamics of regional demographic, socio-cultural, economic, and environmental change (Tsiourtis 2001). Therefore, understanding natural climate variability is of great importance. Developing this understanding is difficult from the relatively short available instrumental record. Natural archives such as tree rings and other proxy records can be used to capture information about climate variability on longer time scales (e.g. Hughes 2002; Jones and Mann 2004 and references therein).

One advantage of tree-ring records is their precise dating to the calendar year, which allows them to be compared directly with instrumental records. This provides a powerful tool for developing qualitative and quantitative reconstructions of climate on seasonal to century or longer time scales. They also represent the most geographically widespread proxy records capable of yielding annually resolved time series over the past several centuries (e.g. Touchan et al. 2003; Jones and Mann 2004; Briffa et al. 2004; Esper et al. 2004) and generally possess the highest correlations with instrumental climate data (Jones et al. 1998). Depending upon growth ecology, the annual patterns of tree rings may reflect environmental influences such as precipitation, temperature, streamflow, and the frequency of extreme drought events (Chbouki 1992; Touchan et al. 1999; Hughes et al. 1999; Meko et al. 2001).

Dendroclimatology in the eastern Mediterranean region is still in the initial stages of development. Most studies are recent (Akkemik 2000; Akkemik and Aras 2005; Akkemik et al. 2005; D'Arrigo and Cullen 2001; Hughes et al. 2001; Touchan et al. 1999, 2003, 2004; Touchan and Hughes 1999) with the exception of an earlier work by Gassner and Christiansen-Weniger (1942). This body of work has demonstrated that tree-ring growth is significantly influenced by precipitation at the investigated sites. It is well known that atmospheric circulation has a significant impact on winter precipitation over all or parts of the Mediterranean (e.g. Zorita et al.1992; Corte-Real et al. 1995; Türkeş 1998; Eshel and Farrell 2000; Cullen and deMenocal 2000; Cullen et al. 2002; Eshel et al.2000; Quadrelli et al. 2001; Dünkeloh and Jacobeit 2003; Bartzokas et al. 2003; Fernández et al. 2003; Xoplaki et al. 2000, 2004 and references therein; Türkeş and Erlat 2005). Generally, this connection is less strong during summer as local and/or sub-regional conditions are more important than the large-scale influence (e.g. Türkeş and Erlat 2003).

This study represents the first large-scale systematic dendroclimatic sampling campaign focused on developing chronologies from the species *Cedrus libani*, *Cedrus brevifolia*, *Juniperus excelsa*, *Pinus brutia*, *Pinus nigra*, *Pinus sylvestris*, *Pinus leukodermis*, and *Abies cilicica* in Turkey, Syria, Lebanon, Cyprus, and Greece. We present late spring/summer (May–August) precipitation reconstructions ranging from 115 years to 600 years in length using the above tree-ring chronologies. We also

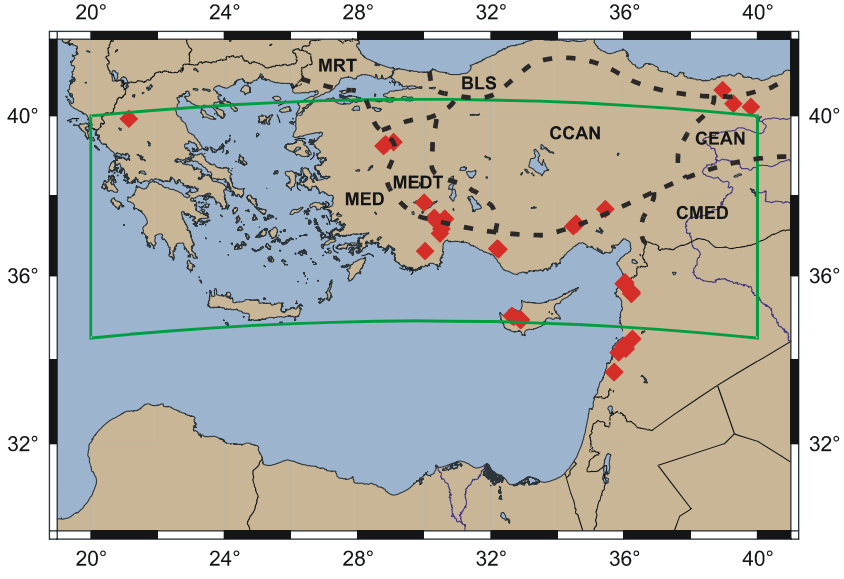

Fig. 1 Locations of tree-ring sites (*filled diamond*). *Solid box* represents the area containing data used in the dendroclimatic reconstructions of precipitation. The climatic classification by Türkeş (1996, 1998), Türkeş et al. (2002) is presented in *dashed lines*

Table 1 Site information for the Eastern Mediterranean region

Site name	Site code	Country	Species	Elevation (m)	Latitude	Longitude	Time span (year)		Total no. of years	No. of trees	No. of cores
							Earliest	Latest			
Yatak Çamı	YAT	Turkey	*Pinus sylvestris*	2213–2278	40°49′N	42°26′E	1757	2001	245	17	34
Eşek Meydanı	ESE		*P. sylvestris*	2305–2388	40°46′N	42°23′E	1613	2001	389	40	72
Gavraz	GAV		*P. sylvestris*	1852	40°40′N	36°57′E	1788	2001	214	14	20
Ayazoğlu mevkii	AYA		*P. sylvestris*	2394–2419	40°37′N	42°30′E	1770	2001	232	20	37
İstasyon mevkii	IST		*P. sylvestris*	1604–2491	40°21′N	42°33′E	1748	2001	254	19	33
Tozlu Tepe	TOZ		*P. sylvestris*	2156–2192	40°18′N	39°16′E	1732	2001	270	15	30
Akyol Deresi	AKY		*P. sylvestris*	2430–2595	40°16′N	42°44′E	1719	2002	284	38	69
Çal Dağı	CAL		*P. sylvestris*	1619–1724	40°14′N	39°05′E	1787	2001	215	16	30
Kirazli	KIR		*Pinus nigra*	1557–1739	39°20′N	29°05′E	1796	2002	207	20	34
Aligalani	ALI		*P. nigra*	1582–1732	39°16′N	28°51′E	1771	2002	232	12	23
Atalani	ATA		*P. nigra*	1453–1499	39°14′N	28°47′E	1792	2002	212	10	19
Circirtepe	CIRP		*P. nigra*	1496–1553	37°38′N	35°26′E	1475	2001	527	18	18
Su Batan	SUB		*Juniperus excelsa*	1808–1916	37°25′N	30°18′E	1246	2000	755	25	36
Aziziye	AZY		*P. nigra*	1601–1670	37°25′N	30°17′E	1511	2001	491	23	35
Dumanli Dağ	DUD		*Pinus brutia*	887–1426	37°24′N	30°38′E	1694	2001	218	21	27
Katrandagi	KAT		*Cedrus libani*	1421–1517	37°23′N	30°36′E	1693	2001	309	23	36
Ananardiç	ANA		*J. excelsa*	1762–1868	37°16′N	34°33′E	1330	2001	672	18	23
Silpişli	SILJ		*J. excelsa*	1727–1851	37°16′N	34°33′E	1350	2001	652	17	22
Neşeli	NESJ		*J. excelsa*	1708–1741	37°12′N	34°28′E	1235	2001	767	24	29
Göller	GOLP		*P. brutia*	1002–1093	37°09′N	30°31′E	1695	2001	308	22	35
Göller	GOLJ		*J. excelsa*	1002–1093	37°05′N	30°31′E	1152	2000	849	16	31
Bayat Bademleri	BAB		*P. brutia*	641–754	37°02′N	30°28′E	1738	2001	264	15	15
Kozlu Pinari	KOP		*P. nigra*	1597–1669	36°39′N	32°12′E	1586	2000	415	16	24
Yellic Beli	YEB		*C. libani*	1668–1779	36°39′N	32°11′E	1628	2000	373	16	24
Elmali	ELMJ		*J. excelsa*	1853–2022	36°36′N	30°01′E	1032	2001	970	44	63
Elmali	ELMC		*C. libani*	1853–2022	36°36′N	30°01′E	1449	2001	553	50	70
Atera	ATEP	Syria	*P. brutia*	409–462	35°50′N	36°01′E	1892	2001	110	7	7
Bait Hamik	BAIP		*P. brutia*	459–565	35°47′N	35°59′E	1882	2001	120	21	25
Mafrak Bait Ablak	MBAP		*P. brutia*	553–560	35°47′N	36°01′N	1901	2001	101	10	11
Kumat Bani Mata	KNM		*C. libani*	1423–1471	35°36′N	36°13′E	1837	2001	165	19	20
Bedayat Al Khandak Al Tawil	BKTA		*Abies cilicica*	1401–1416	35°34′N	36°12′E	1830	2001	172	16	17
Rawisat Almedeki	RWIA		*A. cilicica*	1476–1493	35°33′N	36°12′E	1795	2001	207	17	18
Wadi Balat	WAB	Lebanon	*A. cilicica*	1156–1192	34°28′N	36°14′E	1722	2001	280	16	19
Herch Ehden	HCH		*C. libani*	1617–1664	34°18′N	35°59′E	1809	2001	193	21	22
Bsheri	BSH		*C. libani*	1826–1975	34°14′N	36°02′E	1382	2002	621	46	69
Arz Jaj	ARJ		*C. libani*	1605–1979	34°08′N	35°49′E	1778	2002	225	39	52
Barouk	BAR		*C. libani*	1738–1812	33°41′N	35°41′E	1829	2002	174	18	31
Maaser	MAA		*C. libani*	1693–1734	33°40′N	35°41′E	1730	2002	273	12	19
Stavzos Psokas	STP	Cyprus	*P. brutia*	1040–1082	35°01′N	32°38′E	1739	2002	264	20	38
Tripylos	TRI		*Cedrus brevifolia*	1392–1401	34°59N	32°40′E	1532	2002	471	22	42
Chionistra	CHI		*P. nigra*	1747–1795	34°56′N	32°52′E	1379	2002	624	22	44
Armiantos	AMIB		*P. brutia*	1483–1646	34°55′N	32°54′E	1584	2002	419	17	33
	AMIN		*P. nigra*	1618–1666	34°55′N	32°54′E	1554	2002	449	19	38
Valia Kalda	VKAN	Greece	*Pinus leukodermis*	1639–1729	39°55′N	21°09′E	1407	2003	597	20	40
	VKAL		*P. nigra*	1692–1714	39°54′N	21°10′E	1232	2003	772	21	52

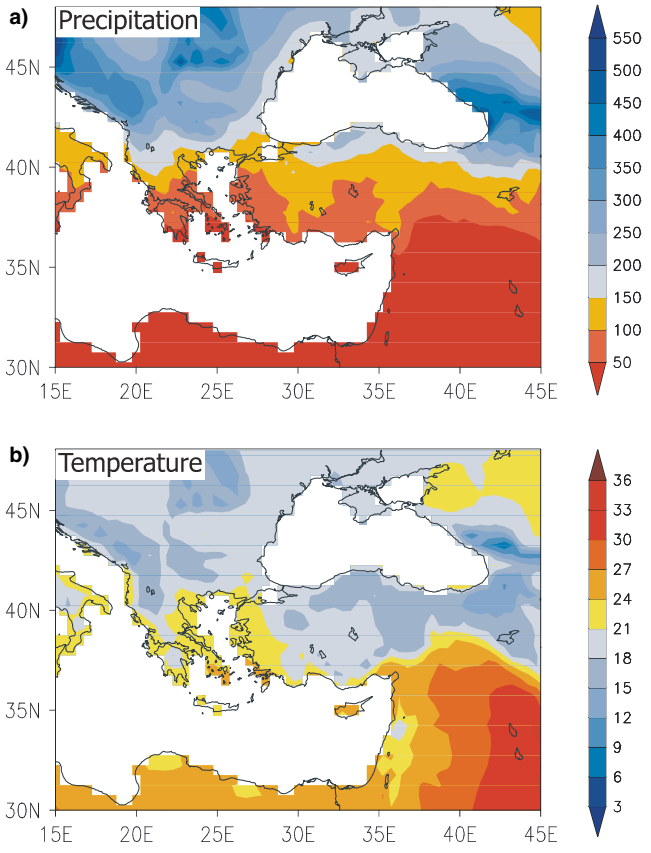

Fig. 2 May–August total precipitation (mm) and temperature (°C) over the eastern Mediterranean, 1948–2000 based on the gridded Mitchell et al. (2004) data

diagnose large-scale climate influences in the tree-ring data for the instrumental and reconstruction periods.

2 Site and climate descriptions

Forty-two tree-ring sites sampled from Turkey, Syria, Lebanon, Cyprus, and Greece are presented in Fig. 1 and Table 1. The sites range in elevation from 400 m to 2,400 m a.s.l. May–August precipitation was found to be the most important seasonal predictor for tree-ring growth in the region (see Results section). In the following section, we briefly describe climate conditions over the study area with emphasis on the May–August season. Figure 2 presents (a) the May–August total precipitation and (b) the May–August mean temperature using the gridded data of Mitchell et al. (2004) over the investigated area for the period 1948–2000.

2.1 Climates of Turkey

The tree-ring sites in Turkey (Table 1) are located in four rainfall regions based on the classification by Türkeş (1996, 1998), Türkeş et al. (2002). These are the Mediterranean climate region (MED) which includes the sites: BAB, ALI, ATA, KIR, ELMJ, ELMC, GOLP, GOLJ, KOP, YEB, and ARAJ; the transition zone between the Mediterranean and the Mediterranean Transition-Mediterranean to Central Anatolia regions (MED-MEDT) which includes the sites: AZY, DUD, KAT, and SUB; the Continental Central Anatolia region (CCAN) which includes the sites: CIRP, ANA, SIL, NESJ, and GAV; and the Continental Eastern Anatolia region (CEAN) which includes the sites: AKY, AYA, CAL, ESE, IST, TOZ, and YAT.

The MED region is characterized by dry, hot, summers and cool, rainy, winters (Türkeş 1996; Türkeş et al. 2002). Precipitation follows a strong seasonal pattern, with the most rainfall occurring during the cold season and very low amounts during the summer. Total annual rainfall is around 750 mm while total May–August rainfall is 50–100 mm (Fig. 2a). Wintertime seasons are characterized by a water surplus, and warm seasons by water deficits. Generally, summer dryness is associated with large-scale regional climate (i.e., the Mediterranean macro-climate) that is controlled by both mid-latitude and North African-Asiatic tropical (e.g. monsoon low) pressure systems (Türkeş and Erlat 2003). The MED-MEDT region is similar to the Mediterranean region with moderately rainy winters and springs. The May–August precipitation is 100–150 mm (Fig. 2a) with annual precipitation of 520 mm.

Cool rainy springs, cold rainy winters, and warm and fairly dry summers characterize the semi-arid and dry semi-humid steppe climate of the CCAN region. May–August precipitation is 100–200 mm (Fig. 2a) with annual precipitation of 400 mm. The sites under the CEAN region conditions have cool rainy springs, early summers and very cold and snowy winters. The climate can be characterized as dry semi-humid and semi-humid steppe and highland. Average May–August precipitation is 150–300 mm (Fig. 2a) with an annual rainfall of 460 mm. The May–August mean temperature in Turkey ranges between 15°C and 27°C (Fig. 2b). At high elevations cooler summers (eastern Turkey) contribute to the lower temperatures. Closer to the Mediterranean Sea, where the role of orography is reduced, higher annual temperatures are observed.

2.2 Climates of Syria, Lebanon, and Cyprus

The study areas located in Syria, Lebanon, and Cyprus are characterized by a Mediterranean climate with a typical seasonal rhythm of long, hot and dry summers and cool, rainy winters. Most precipitation occurs from fall through spring, with summers being fairly dry. Most of the sites, due to their high elevation, are covered with snow from December through April. May–August precipitation ranges between 0 mm and 100 mm (Fig. 2a) with annual precipitation ranging between 500 mm and 1,400 mm.

Higher mean May–August temperatures characterize the lower elevations of these countries. Values range

Table 2 Summary statistics for the 36 chronologies for the ARSTAN program

Chronology name	Site code	Total chronology			Kurtosis	Common intervals			
		Mean sample segment length	Standard deviation	Skewness		First year SSS[a] > 0.85	Time span	Mean correlation among radii	Explained variance PC1 (%)
YatakÇamı	YAT	186	0.13	0.21	0.79	1803	1853–2001	0.32	35
Eşek Meydanı	ESE	239	0.14	0.48	1.07	1682	1837–2001	0.34	36
Gavraz	GAV	170	0.16	0.22	0.10	1804	1812–2001	0.48	49
Ayazoğlu mevkii	AYA	175	0.12	0.02	0.19	1802	1857–2001	0.33	35
İstasyon mevkii	IST	144	0.11	−0.13	0.57	1846	1905–2001	0.26	29
Tozlu Tepe	TOZ	166	0.15	0.65	0.55	1799	1885–2000	0.47	50
Akyol Deresi	AKY	200	0.12	−0.07	1.00	1757	1855–2001	0.35	35
Çal Dağı	CAL	150	0.17	0.28	1.18	1836	1890–1997	0.32	35
Northwest[b]	ALI-ATA- KIR	172	0.17	0.21	0.14	1799	1851–2001	0.37	38
Circirtepe	CIRP	390	0.20	0.40	3.82	1577	1689–2001	0.37	41
Su Batan	SUB	299	0.18	0.12	0.14	1338	1672–1950	0.44	50
Aziziye	AZY	204	0.13	0.08	0.00	1789	1861–2000	0.31	34
Dumanli Dağ- Göller[c]	DUD-GOLP	159	0.16	0.32	0.29	1793	1890–1999	0.41	42
Katrandagi	KAT	157	0.18	0.17	0.20	1815	1878–2000	0.47	49
South Central[d]	ANA-NESJ- SILJ	289	0.20	0.19	0.14	1353	1823–1998	0.41	44
Göller	GOLJ	341	0.16	0.14	0.49	1594	1759–2000	0.32	36
Bayat Bademleri	BAB	171	0.19	−0.50	0.25	1751	1797–1996	0.59	65
Kozlu Pinari	KOP	295	0.15	0.24	0.91	1682	1744–2000	0.31	35
Yellic Beli	YEB	200	0.19	0.18	0.26	1743	1818–2000	0.36	41
Elmali	ELMJ	309	0.19	0.34	0.19	1470	1820–2000	0.37	40
Elmali	ELMC	330	0.17	−0.40	1.21	1505	1759–1997	0.48	50
PIBR Forest-SYR[e]	ATEP-BAIP- MBAP	89	0.13	−0.39	0.08	1909	1937–2000	0.20	24
Kumat Bani Mata	KNM	99	0.20	0.16	0.04	1883	1921–2001	0.36	41
ABCE Forest-SYR[f]	BKTA_RWIA	110	0.25	0.77	2.86	1872	1913–2000	0.26	31
Wadi Balat	WAB	137	0.14	−0.22	0.44	1876	1913–2001	0.22	28
Herch Ehden	HCH	138	0.18	1.41	11.93	1857	1891–1990	0.40	43
Bsheri	BSH	253	0.22	0.33	3.51	1548	1807–1964	0.42	44
Arz Jaj	ARJ	113	0.18	0.18	2.51	1874	1924–2001	0.33	36
Barouk	BAR	116	0.24	2.00	11.81	1870	1899–2002	0.37	41
Maaser	MAA	156	0.24	−0.19	1.04	1821	1880–2002	0.49	53
Stavzos Psokas	STP	213	0.16	−0.02	1.15	1765	1829–2002	0.37	39
Tripylos	TRI	238	0.18	0.64	3.56	1743	1812–2002	0.37	39
Chionistra	CHI	332	0.19	0.62	0.81	1596	1727–2002	0.41	44
Armiantos	AMIB	229	0.18	0.16	0.81	1706	1803–2002	0.42	45
	AMIN	325	0.14	0.16	0.61	1591	1640–1934	0.30	33
Valia Kalda	VKAN-VKAL	358	0.22	0.27	0.87	1308	1707–2002	0.42	44

[a]SSS is Subsample Signal Strength (Wigley et al. 1984)
[b]Northwest combines Kirazli, Aligalani, and Atalani into one chronology (see text)
[c]Dumanli Dağ- Göller combines DUD and GOLP into one chronology (see text)
[d]South Central combines Neşeli, Anarndiç and Silpişli into one chronology (see text)
[e]PIBR Forest-SYR combines Atera, Bait Hamik, and Mafrak Bait Ablak (see text)
[f]ABCE Forest-SYR combines Bedayat Al Khandak Al Tawi and Rawisat Almedeki (see text)

between 18°C and 28°C, indicating a slightly warmer summer climate than Turkey (Fig. 2b).

Summer conditions over the eastern Mediterranean are highly persistent, particularly during the July–August period. The lower levels of the atmosphere are dominated by the Persian trough (Alpert et al. 1990; Bitan and Saaroni 1992; Saaroni et al. 2003; Ziv et al. 2004), a surface low-pressure trough extending from the Asian monsoon through the Persian Gulf, and along southern Turkey to the Aegean Sea. The combination of the sub-tropical high of the Azores and the Persian trough leads to northwesterly (Etesian) winds. The Etesian winds are connected with a continual cool advection from Eastern Europe and the Mediterranean into the Levant (e.g., Saaroni et al. 2003; Ziv et al. 2004).

In contrast, a persistent warming by subsidence, which dominates the eastern Mediterranean, counteracts the advective cooling over the region (Saaroni et al. 2003; Ziv et al. 2004, 2005). Ziv et al. (2004) report on a first-order effect that has direct control of the Asian monsoon on the interdiurnal variations of the vertical motion over the Levant and a second-order effect that controls the concurrent variations of the Etesian winds and the subsidence.

2.3 Climate of the Greek sites

The sites in Greece are located in the northern mainland, which has a modified continental Mediterranean climate. This regime combines an equal annual rainfall distribution plus the influence of Mediterranean seasonal variability. Total May–August precipitation over the area reaches 150 mm (Fig. 2a), though highly variable, with an annual rainfall of 500 mm. Temperatures vary with elevation, remaining below 20°C at upper altitudes (Fig. 2b). Warm anomaly conditions over Greece occur when warm air dominates over the eastern Mediterranean, in connection with an anomalous northeasterly-to-easterly flow and subsidence at the upper levels. This leads to increased stability and inhibition of convection, resulting in clear skies and maximum insolation conditions. Such a combination favors a temperature structure with land–sea contrasts due to the higher heat capacity of the water masses and faster thermal response of the land (Xoplaki et al. 2003a).

3 Data

3.1 Tree-ring data and chronology development

Thirty-six chronologies from 42 sites were developed from Turkey, Syria, Lebanon, Cyprus, and Greece (Table 2). The dominant tree species in the study areas are shown in Table 1. Samples were collected from species known to share a high degree of common variation that is strongly driven by climate. Increment cores were taken at all sites and full cross-sections were taken from stumps of cedar and juniper. Samples were fine-sanded and crossdated using standard dendrochronological techniques (Stokes and Smiley 1996; Swetnam 1985). The width of each annual ring on the cores and cross-sections was measured to the nearest 0.01 mm.

Each series of tree-ring width measurements was fit with a 67% cubic smoothing spline with a 50% cutoff frequency to remove non-climatic trends due to age, size, and the effects of stand dynamics (Cook and Briffa 1990). The de-trended series were then pre-whitened with low-order autoregressive models to remove persistence not related to climatic variations. The individual indices were combined into single averaged chronologies for each combination of site and species using a bi-weight robust estimate of the mean (Cook 1985). Since visual crossdating and computer-based quality control showed a strong similarity among the following sites, they were combined to form single chronologies: (1) South Central combines Neşeli (NESJ), Ananrdiç (ANA), and Silpişli (SIL); (2) Northwest combines Kirazli (KIR), Aligalani (ALI), and Atalani (ATA); (3) Dumanli Dağ-Göller combines Dumanli Dağ (DUD) and Göller (GOLP); (4) PIBR Forest-SYR combines Atera (ATEP), Bait Hamik (BAIP), and Mafrak Bait Ablak (MBAP); and (5) ABCE Forest-SYR combines Bedayat Al Khandak (BKTA) and Rawisat Almedeki (RWIA).

3.2 Climate data

Two gridded climate data sets were used for this study: (1) Monthly precipitation and temperature records were obtained from the high resolution 0.5° gridded climate dataset CRU TS 2.0 (Mitchell et al. 2004). A gridded region defined by latitudes 30°N–45°N and longitudes 20°E–40°E was selected as the initial total universe of possible historic climate data. This region is larger than the core area defined by the location of the tree-ring sites so that regional, as well as local, climate effects on tree growth could be detected. Climate data for the land areas within this gridded network were available for 823 of the 1,200 total individual grid points. The period 1931–2000 was chosen for analyses because it maximizes the number of station records used in constructing the gridded climate network while optimizing stability and consistency in sample depth.

Monthly (January through December), seasonal (e.g. winter, spring, summer, fall), and annual total precipitation and mean temperature datasets were developed for each of the 823 available grid points. Monthly data from multiple grid points were used to build a library of varying sized gridded climate networks. From this, seasonal and annual total precipitation and mean temperature data were created for each of the climate grids. All these data (from the individual and combined grid points) were used in evaluating the climate–tree growth relationship. For our analysis we defined the gridded

region latitudes 34.5°N–40°N and longitudes 20°E–40°E as the most appropriate window.

(2) Gridded (2.5°×2.5° latitude–longitude resolution) monthly sea level pressure (SLP) data and geopotential heights at different levels (850, 700, 500 and 300 hPa) for the period 1948 to 2000 were taken from the NCEP/NCAR reanalysis data sets (Kalnay et al. 1996; Kistler et al. 2001). In order to isolate those characteristics of atmospheric variability related to the tree-ring data, a spatial window was defined based on the highest correlation between the first principal component of the 36 tree-ring width data set and the large-scale Northern Hemisphere geopotential height fields and SLP. It was found that the geographical window spanning from 40°W–90°E and 20°N–70°N provided the most suitable atmospheric information for use with the tree-ring indices.

4 Methods

4.1 Response function analysis

Response function analysis (Fritts 1976; Fritts and Guiot 1990; Fritts and Shashkin 1995) was conducted between the 0.5° gridded climate data (temperature and precipitation, see Sect. 3.2) and the tree-ring chronologies. Candidate predictors were monthly temperature and precipitation values for the 14 months ending in October of the year of growth. Predictands were: (1) tree-ring chronologies from the individual countries, (2) tree-ring chronologies built from each species (in total and by country), and (3) chronologies of different lengths were developed (described in Sect. 4.2). These predictands were tested against the nearest individual grid points and averages of numerous combinations of the climate data (predictors).

4.2 Precipitation reconstructions

The response function analysis identified May–August total precipitation as the most appropriate seasonal predictand for reconstruction (not shown) based on consistent patterns of monthly series with significant response function elements of the same sign. The precipitation reconstructions were calibrated on the mean May–August precipitation of the box shown in Fig. 1, covering latitudes 34.5°N–40°N and longitudes 20°E–40°E. Six separate reconstructions were developed to accommodate the varying chronology lengths and to test the stability of the model: 1400–2000 (seven chronologies), 1500–2000 (nine chronologies), 1600–2000 (14 chronologies), 1700–2000 (18 chronologies), 1800–2000 (32 chronologies) and 1885–2000 (36 chronologies).

The different chronology sets were transformed to uncorrelated predictors by projecting them to their principal components (PCs) prior to developing the regression equation. Predictors for the final reconstruction models were selected from the PCs by a forward stepwise regression procedure. For the 1885–2000, 1800–2000, 1700–2000, 1600–2000, 1500–2000, and 1400–2000 reconstructions, regression against the first PC accounts for 52, 49, 41, 37, 41, and 40%, respectively of the variance of May–August precipitation, and entered as

Table 3 Results of the statistical calibrations between May – August precipitation and tree growth for six reconstructions

Reconstruction	Calibration Period	Verification Period	Variable	Coefficient	F Value	P	Adjusted-R^2 Calibration	R^2 Verification	Reduction of Error, RE
1885–2000	1966–2000	1931–1965	Constant	77.12	29.49	0.0001	0.46	0.57	0.58
			PC1	−5.18					
1800–2000			Constant	77.16	25.72	0.0001	0.42	0.54	0.54
			PC1	−5.02					
1700–2000			Constant	76.82	19.50	0.0001	0.35	0.46	0.46
			PC1	−5.52					
1600–2000			Constant	76.62	17.06	0.0001	0.32	0.41	0.42
			PC1	−5.79					
1500–2000			Constant	77.41	17.12	0.0001	0.32	0.47	0.46
			PC1	−7.31					
1400–2000			Constant	77.56	18.65	0.0001	0.34	0.45	0.45
			PC1	−8.29					
1885–2000	1931–1965	1966–2000	Constant	78.48	44.19	0.0001	0.56	0.47	0.48
			PC1	−5.29					
1800–2000			Constant	78.42	37.89	0.0001	0.52	0.42	0.45
			PC1	−5.12					
1700–2000			Constant	78.21	28.03	0.0001	0.44	0.37	0.38
			PC1	−5.79					
1600–2000			Constant	78.17	23.25	0.0001	0.40	0.34	0.34
			PC1	−6.45					
1500–2000			Constant	77.79	29.31	0.0001	0.45	0.34	0.34
			PC1	−8.90					
1400–2000			Constant	76.58	27.04	0.0001	0.43	0.36	0.37
			PC1	−9.27					

the single most significant predictor for each of the reconstructions.

Calibration equations were developed using precipitation data (predictand) for the period 1931–2000. The PRESS procedure was used for cross-validation (Weisberg 1985; Fritts et al. 1990; Meko 1997; Touchan et al. 1999, 2003) in order to maximize the number of observations and degrees of freedom used to calculate model significance in the final regression equation. This measure is calculated by sequentially removing single observations from the calibration period and calculating a new regression equation over the remaining n-1 observations and using the equation to estimate the observation that was removed. This is repeated for each of the n observations. In order to verify model stability, a split-sample procedure (Snee 1997; Meko and Graybill 1995; Touchan et al. 2003) that divided the full period into two subsets of equal length (1931–1965 and 1966–2000) was used (Table 3). The reduction of error statistic (RE; Cook et al. 1994) was used to test whether there was skill beyond what could be derived by simply using the calibration period mean as the reconstruction (Fritts 1976). This test is passed if the RE value is positive. The resulting models for the period 1931–2000 were then used to calculate the six reconstructions from the chronology sets.

4.3 Analysis of extreme dry and wet events

Runs analysis (Dracup et al. 1980), a non-parametric test of whether consecutive values above or below a defined threshold are random, was used on the reconstructions to study extreme May–August drought and wet events. Empirical thresholds for the dry and wet events were defined as 90% (70 mm) and 110% (85 mm) of the 1931 to 2000 mean observed May–August precipitation, respectively (Touchan et al. 2003, 2004).

4.4 Large-scale circulation patterns

4.4.1 Canonical correlation analysis in the empirical orthogonal functions space

We follow the same approach as Xoplaki et al. (2003b, 2004) relating Mediterranean summer temperature and wet season precipitation to large-scale atmospheric circulation dynamics. A downscaling model is calibrated using canonical correlation analysis (CCA) in the empirical orthogonal function (EOF) space. We provide here a short overview of these methods. The reader is referred to the detailed descriptions provided by Barnett and Preisendorfer (1987), Wilks (1995) and von Storch and Zwiers (1999).

Canonical correlation analysis is an appropriate method to search for linear relationships between two space/time dependent variable sets. The CCA selects pairs of spatial patterns of each variable set such that the (time dependent) pattern amplitudes are optimally correlated. The canonical time series describe the strength and sign of the corresponding pattern for each realization in time. Here, canonical series are normalized to unit variance and the canonical correlation vectors (patterns) represent typical anomalies in the units of the variable with respect to its mean state. The correlation between the canonical series measures the degree of association between the canonical patterns of predictor and predictand variables.

Prior to CCA the original data are usually projected onto their EOFs, retaining those that account for most of the total variance and minimize noise. As a preliminary step to the EOF calculation, the annual cycle was removed from all grid point time series by subtracting the respective month's 1931–2000 mean from each monthly value. In order to account for latitudinal distortions in the grid area, the gridded predictor data were weighted by multiplying them with the square root of the cosine of their latitude (North et al. 1982; Livezey and Smith 1999). A second step to ensure the stationarity of the variables needed for calculating EOFs and subsequent CCA involved removal of the linear trend of the time series (standard least square fit, e.g. Edwards 1984).

After the diagonalisation of the covariance and cross-correlation matrices during EOF and CCA processes, the long term trends were recovered by projecting (regressing) the original datasets onto their EOFs (canonical vectors), thus providing estimations of the principal components and canonical series with long term variability and trends (e.g. Xoplaki et al. 2003a, b, 2004). To determine the most suitable number of EOFs to retain from the predictor field and predictand time series, various CCA analyses with different numbers of retained EOFs were performed. The first eight precipitation principal components were selected to perform the subsequent CCA analysis in combination with the principal components of the predictand field (i.e. tree-ring indices).

We performed different EOF-CCA experiments relating precipitation and temperature, as well as various large-scale circulation fields (300, 500, 700, and 850 hPa, SLP), with the tree-ring indices. We also tested different combinations of the months and seasons which account for the highest amount of explained variance of the tree-ring data. May–August precipitation proved to be the most important predictor, explaining approximately 22% of the total variability in the tree-ring indices. A multiple CCA using several predictors (temperature and precipitation or circulation fields at different levels) did not improve the explained variance (not shown).

4.4.2 Linear regression analysis

Regression maps have been used in several studies to identify large-scale climate signals associated with given time series such as identifying precipitation and tem-

perature signals connected with the Arctic and North Atlantic Oscillations (e.g. Hurrell 1996; Thompson and Wallace 1998; Shindell et al. 1999) and large-scale atmospheric variables related to Mediterranean summer air temperature (Xoplaki et al. 2003a, b). If the link between the time series and the space-time-dependent field is formulated individually for each location, regression maps (which are a collection of individual regression coefficients) are a straightforward way to capture the signal of the time series in the space-time-dependent field (e.g. Widmann 2004).

For our purposes, it is of interest to understand the influences on tree-ring indices variability for the eastern Mediterranean region during the May–August season over the last few decades. Since precipitation proved to be the most important predictor, we are mainly interested in explaining the rainfall variability represented in the first CCA by regressing its time series to the large-scale atmospheric circulation at sea level, at different upper levels, and gridded air temperature. With the first CCA time series, large-scale patterns are generated by computing the regression slope coefficients between the CCA time series of the May–August precipitation and the time series of May–August 300, 500, 700, and 850 hPa, SLP, and surface air temperature from each point in the data set.

4.4.3 *Composite analysis*

We also used composite analysis to extract information regarding the large-scale climate SLP and surface air temperature signals contained in the eastern Mediterranean tree-ring indices and extreme high and low reconstructed precipitation both for the instrumental period and back to 1764. For this, we reconstructed SLP and surface air temperature fields as described by Luterbacher et al. (2002, 2004) though using only station pressure (station temperature) series. The SLP and surface air temperature fields are independent (i.e. they share no common predictor in the reconstruction procedure). Since summer SLP fields can be considered reliable from 1764 (not shown), we restricted our composite analysis to the last 237 years.

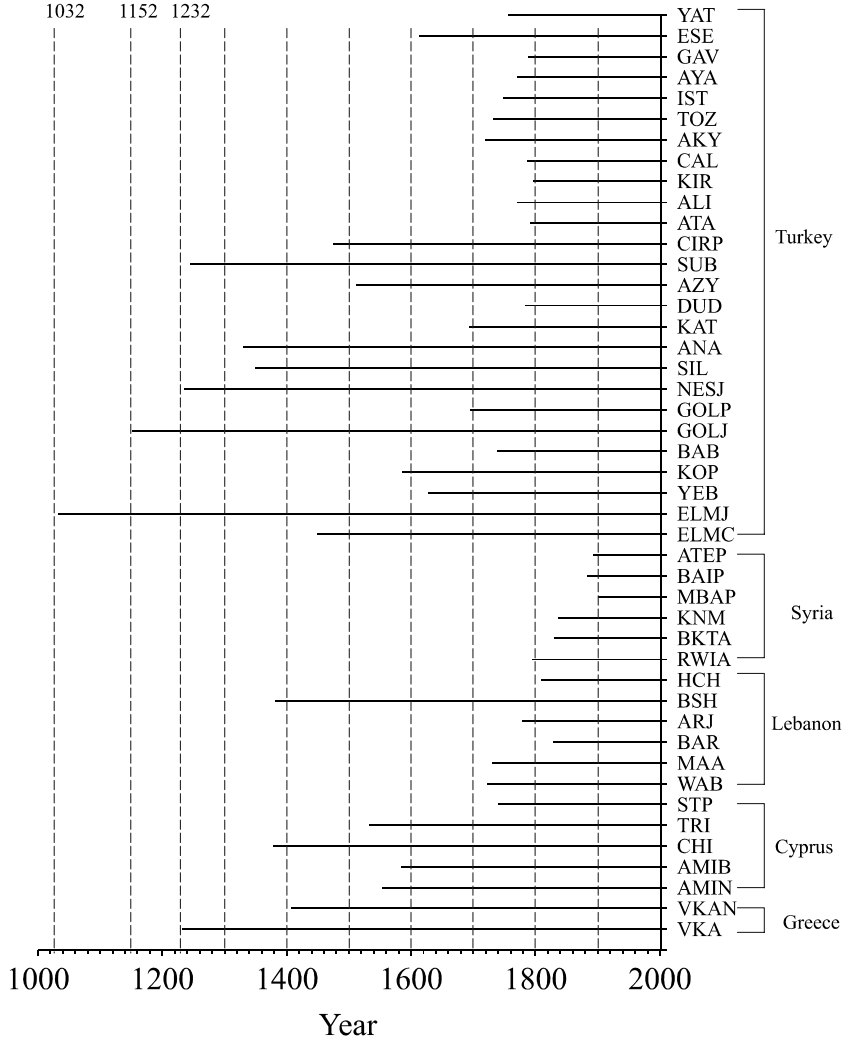

Fig. 3 Time coverage of the chronologies. *Each horizontal line* marks the time span of the chronology whose letter code appears by the *right-hand scale*

The composite technique involves identifying coherent structures in the SLP, geopotential height, and near surface air temperature fields that are associated with below and above normal reconstructed precipitation. Common composite analyses are given as means with some form of statistical significance test to assess chance occurrence of the pattern. These analyses have at least two shortcomings (Brown and Hall 1999): (1) the mean (as a measure of location) is not resistant to the effects of outliers, especially in small samples and (2) it does not account for the associated variance. For these reasons we applied the recently presented scaled mean and modified t values that are particularly useful for small samples or in cases where the data distribution is unknown or known to be non-Gaussian (Brown and Hall 1999).

We conducted two composite analyses: The first was based on the first CCA, where we selected the positive and negative precipitation canonical scores with the threshold of one standard deviation and calculated the anomaly composite for the corresponding upper, middle and lower tropospheric atmospheric fields, SLP, surface air temperature, and precipitation for the period 1948–2000 (for which NCEP Reanalysis data are available). For the second, we used the driest and wettest eastern Mediterranean summers over the last 237 years that exceed 1.5 standard deviations from the mean and plotted the corresponding SLP and surface air temperature anomaly patterns.

4.4.4 Running correlation analysis

Running correlation analysis (computed in moving windows) is frequently used in climate research to diagnose changes in relationships between two circulation indices (e.g. Schmutz et al. 2000; Jacobeit et al. 2001, 2003; Gershunov et al. 2001; Slonosky et al. 2001; Slonosky and Yiou 2002; Jones et al. 2003; Timm et al. 2004). At lower frequencies, the relationships between any pair of observed interannual climate modes are expected to fluctuate in a purely stochastic manner. Although some of this modulation may have a physical basis and be predictable, most of it may be stochastic and, therefore, unpredictable (Gershunov et al. 2001). A 30-year running correlation analysis between the first and second EOF (which together account for approximately 55% of total variance of European summer SLP) of SLP (Luterbacher et al. 2002) and precipitation series were calculated for the period 1764–2000. Significance levels were estimated from 1,000 Monte Carlo simulations of independent white noise processes.

5 Results and discussion

5.1 Tree-ring chronologies

The lengths of the 36 combined chronologies (derived from the 42 site collections) range from 115 (PIBR Forest-SYR, Syria) to 970 years (Elmali, Turkey; Table 1 and Fig. 3). Statistical analyses of each chronology are summarized in Table 2. The mean correlation among individual radii at each site represents the strength of their common signal and ranges from 0.26 to 0.59. The highest correlation is for Bayat Bademleri (Turkey) and the lowest is for the chronology developed from Bedaya, Al Khandak, Al Tawi and Rawisat Almedeki (Syria).

The mean sample segment length (MSSL) of the 36 chronologies ranges from 89 years to 390 years. Half of these chronologies have MSSL greater than 200 years in length and many have several samples that exceed 400 years. For the chronologies used to develop the 1400–2000 reconstruction, MSSL for BSH, south central, SUB, ELMJ, CHI, GOLJ, and VKAN-VKAL are 253, 289, 299, 309, 332, 338, and 358 years, respectively. In each of these chronologies 10–35% of the samples are greater than 400 years in length. Therefore, the chronologies are suitable for investigating low-frequency (that is, centennial) climate variability.

Principal components analysis was used to capture the regional dendroclimatic signal and provide an understanding of how the chronologies filter their

Table 4 Results of the statistical calibrations and cross-validation between May – August precipitation and tree growth for six reconstructions

Reconstructions	Calibration Period	Variable	Coefficient	F Value	P	Adjusted-R^2 calibration	PRESS	No. of chronologies
1885–2000	1931–2000	Constant	77.78	76.92	0.0001	0.52	0.50	36.00
		PC1	−5.22					
1800–2000		Constant	77.77	66.63	0.0001	0.49	0.46	32.00
		PC1	−5.05					
1700–2000		Constant	77.46	49.93	0.0001	0.42	0.38	18.00
		PC1	−5.64					
1600–2000		Constant	77.27	42.22	0.0001	0.37	0.34	14.00
		PC1	−6.10					
1500–2000		Constant	77.43	48.11	0.0001	0.41	0.38	9.00
		PC1	−8.18					
1400–2000		Constant	77.00	47.93	0.0001	0.41	0.38	7.00
		PC1	−8.87					

Table 5 Pearson correlation coefficient ($p = 0.0001$) between the different reconstructions

Reconstructions	1400–2000	1500–2000	1600–2000	1700–2000	1800–2000
1500–2000	0.97				
1600–2000	0.92	0.96			
1700–2000	0.91	0.95	0.99		
1800–2000	0.87	0.91	0.94	0.97	
1885–2000	0.87	0.91	0.93	0.96	0.99

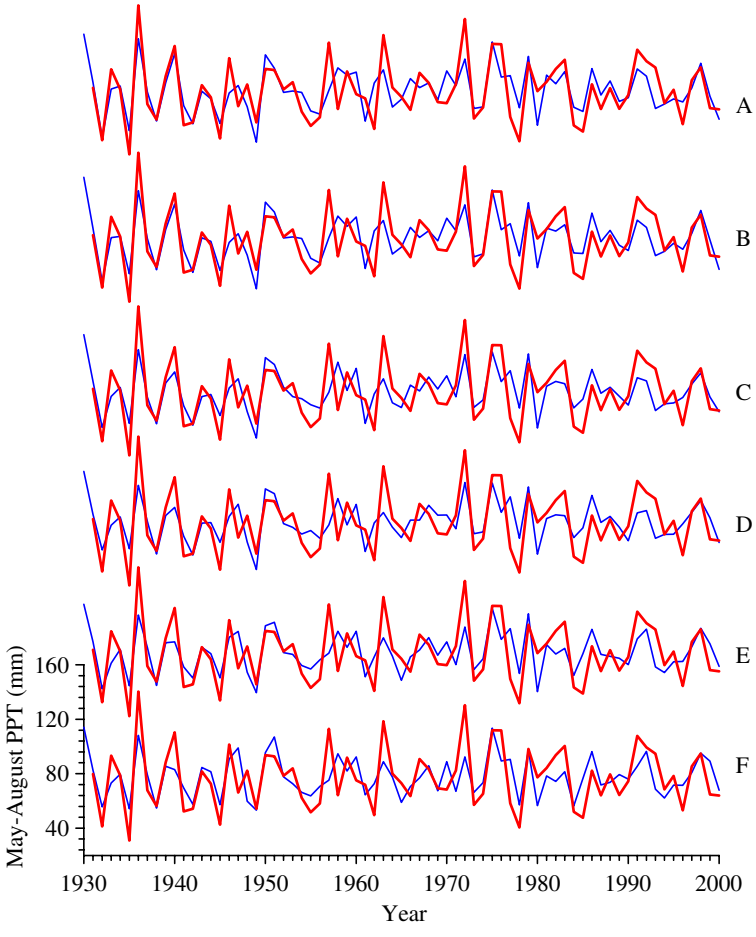

Fig. 4 Comparison of actual (*red line*) and estimated May–August precipitation (*blue line*) for the 1931–2000 period. **a** 1885–2000 reconstruction, based on 36 chronologies; **b** 1800–2000 reconstruction, based on 32 chronologies; **c** 1700–2000 reconstruction, based on 18 chronologies; **d** 1600–2000 reconstruction, based on 14 chronologies; **e** 1500–2000 reconstruction, based on nine chronologies; **f** 1400–2000 reconstruction, based on seven chronologies

respective climatic signals. PC1 accounts for 35% of the common tree-ring variance for the 1885–2000 data set (where all the chronologies were included in the analysis). PC1 shows strong positive weights throughout the region, especially in southern Turkey and Cyprus. PC2 (accounting for 9% of the variance) shows the contrast between northeastern Turkey and Syria and Lebanon (not shown).

The 36 chronologies are well replicated from trees growing on sites where their growth is strongly influenced by climatic variability. They represent the first specifically dendroclimatic tree-ring network for this region and indicate the great potential that exists for future work. This spatial network of chronologies contains seasonal precipitation and temperature signals covering a fairly broad geographical area as indicated by the analyses reported here. This provides further evidence of the value for continued and intensified sampling in the eastern Mediterranean region. The chronologies show a common high response to extreme dry and wet May–August precipitation. This synchronicity of strong patterns in tree-ring growth suggests that pan-regional growth forcing mechanisms are responsible.

One of the major objectives of dendroclimatogists is to obtain the longest possible tree-ring records from living and dead trees to investigate climate variability over several centuries or longer. In most cases we were able to collect samples that were several hundred years in length. This was accomplished primarily by applying experience gained in the semi-arid American Southwest in the selection of species, sites, and individual trees for analysis. Furthermore, the MSSL of the chronologies is adequate to investigate centennial climate variability

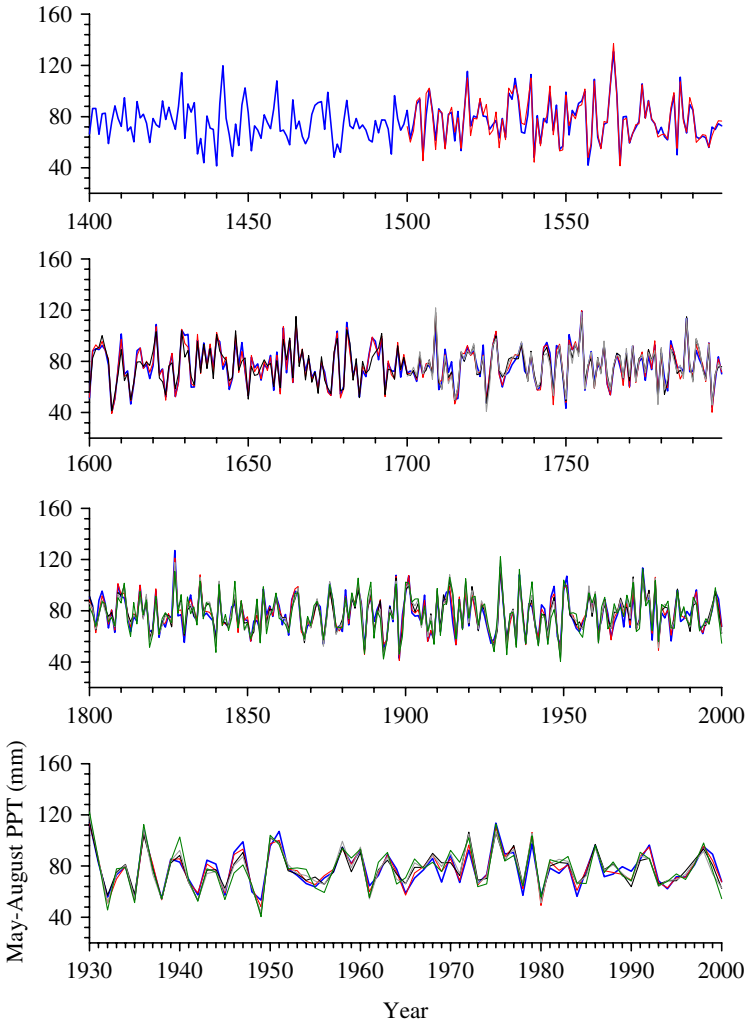

Fig. 5 Time series plots of the six May–August precipitation reconstructions overlaid on the same axes demonstrating similar patterns in high frequency variability

when combined, as here, with conservative de-trending of the individual measurement series.

5.2 Precipitation reconstructions

Final regression statistics for the six reconstructions obtained from the relationship between the first PC of the tree-ring (predictors) and precipitation (predictand) data are highly significant (Table 4). Pearson correlation coefficients among the six reconstructions range between 0.87 and 0.99 (Table 5). Because of the similarity and strength of the derived calibration equations and verification tests, the full calibration period (1931–2000) was used for all reconstructions. This allowed us to retain the maximum variability in the reconstructions (Table 4 and Fig. 4). All subsequent discussion refers to the longest of these reconstructions, that covering the period AD 1400–2000.

This reconstruction is significantly correlated with a February–August precipitation reconstruction developed by D'Arrigo and Cullen (2001) ($r = 0.69$, $n = 353$, $p = 0.001$) for Sivas, central Turkey. A similarly strong relationship was found with reconstructed May–July Standardized Precipitation Index for most of Turkey and adjoining regions (Touchan et al. 2004).

Several major historical events coincide with extreme dry and wet periods seen in the May–August precipitation reconstruction (Kuniholm 1990; Purgstall 1983). Kuniholm (1990) relays historical evidence (H. Inalcik and W. Griswold, personal communication) of a widespread famine and food shortages across Turkey, Syria and Italy during the period of 1590–1595. This is coincident with the longest period of extended extreme drought in the reconstruction (1591–1595). In addition, several other episodes of famine brought on by crop shortages correspond with dry events in the reconstruction. In 1570–1571, when wheat exports were forbidden in the Ottoman Empire, the reconstruction shows evidence of a 2-year dry event. Kuniholm (1990) identified single year short-term events such as a 1579 famine in the Aegean region and Syria and a 1585 famine and drought in west Anatolia and Eastern Asia Minor, both of which correspond to extreme dry events in the reconstruction. He also references a great drought in 1874 in Ankara, Turkey, which resulted in the death

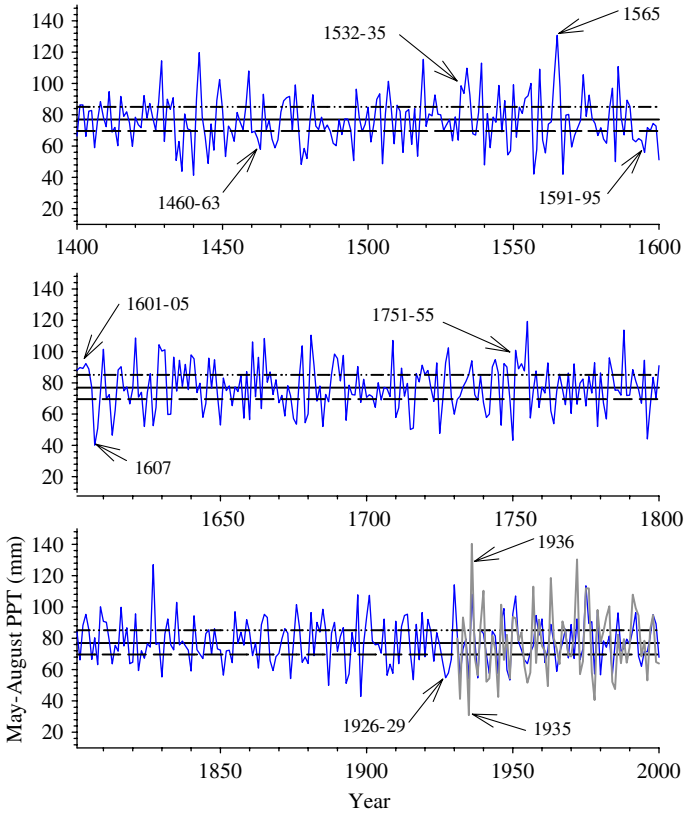

Fig. 6 1400–2000 May–August precipitation reconstruction time series. *Horizontal solid line* is the mean of the observed data. *Horizontal dashed line* is the empirical threshold of 90% of the 1931–2000 mean May–August precipitation (70 mm). *Horizontal dashed-dotted-dashed line* is the empirical threshold of 110% of the 1931–2000 mean May–August precipitation (85 mm). *Solid grey line* is the actual May–August precipitation (Mitchell et al. 2004)

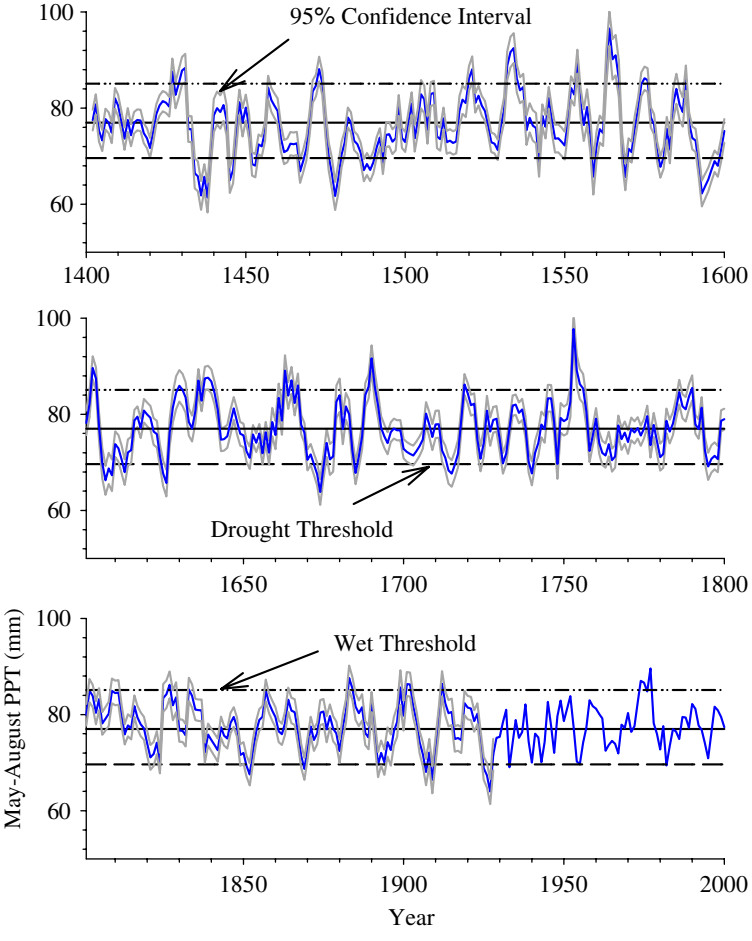

Fig. 7 Five-year moving average of reconstructed May–August precipitation. Values are plotted at the center of each 5 year period. Uncertainty in reconstructed values is shown by two standard errors

of nearly a third of the human population as well as large number of herd animals. This, too, was an extreme event year in the reconstruction.

Purgstall (1983) reported catastrophic fires and famine in Anatolia in 1660. The reconstruction shows indeed that 1660 was an extremely dry summer. In addition, the preceding year was wetter than average. This is a common pattern where during wet years there is a buildup of fine fuels which become an important pre-condition for fire ignition and spread when conditions become drier (Baisan and Swetnam 1990; Swetnam 1993; Touchan et al. 1996). Purgstall (1983) reported a sustained famine in Anatolia from 1925–1928. The reconstruction shows an extended period of 4 years of drought during the same period. It is worth noting that this period of drought ends with one of the wettest years recorded in the reconstruction (1930 is the seventh wettest year identified in the reconstruction).

5.3 Analysis of extreme dry and wet events

The statistics are similar for all reconstructions. Therefore, we restricted the analysis of drought and wet events to the longest reconstruction (1400–2000; Table 5 and Fig. 5). The standard deviations from the mean (77.4 mm) over the calibration period are 14.1 mm for the reconstruction and 22.0 mm for the observed data. The May–August precipitation time series is plotted in Fig. 6. The reconstruction contains 186 dry events with a mean recurrence interval of 3.2 years. The maximum interval between May–August dry periods is 12 years (1517–1529). A total of 97 dry events had a duration of 1 year. Twenty-six dry periods had a duration of 2 years, eight drought events had a duration of 3 years, two drought events had a duration of 4 years (1460–1463 and 1926–1929), and one drought event had a duration of 5 years (1591–1595). The driest year (40 mm) in the reconstruction is 1607. The driest year (31 mm) in the observed May–August precipitation data is 1935. May–August dry periods of 1 year were evenly distributed from 1400 through 1700.

Although there is no visible trend in reconstructed precipitation, there is a notable increase in the frequency of single dry years during the nineteenth and twentieth centuries. Dry periods of 2 years were well distributed from 1500 through 1700. However, these dry periods decline in frequency during the fifteenth, nineteenth, and twentieth centuries. The fifteenth century had the highest number of 3-year dry periods (four events). No 3-year dry periods occurred during the sixteenth and seventeenth centuries.

The extreme drought events of the May–August reconstruction were evaluated against two climate stations, Beirut (Lebanon) and Nicosia (Cyprus), from 1888–1930 to test the strength of the reconstruction. Even though these stations are at low elevations and some distance from the tree-ring sites, the reconstruction correctly identified 5 of the 12 extreme dry events recorded by these stations.

The reconstruction contains 180 May–August wet events with a mean recurrence interval of 3.3 years and a maximum interval of 15 years (1481–1496). The wettest year in the reconstruction was 1565 (131 mm). The wettest year during the instrumental period was 1936 (140 mm). Eighty-six wet events had a duration of 1 year, 22 wet events had a duration of 2 years, eleven wet events had a duration of 3 years, one wet event had a duration of 4 years (1532–1535), and two wet events

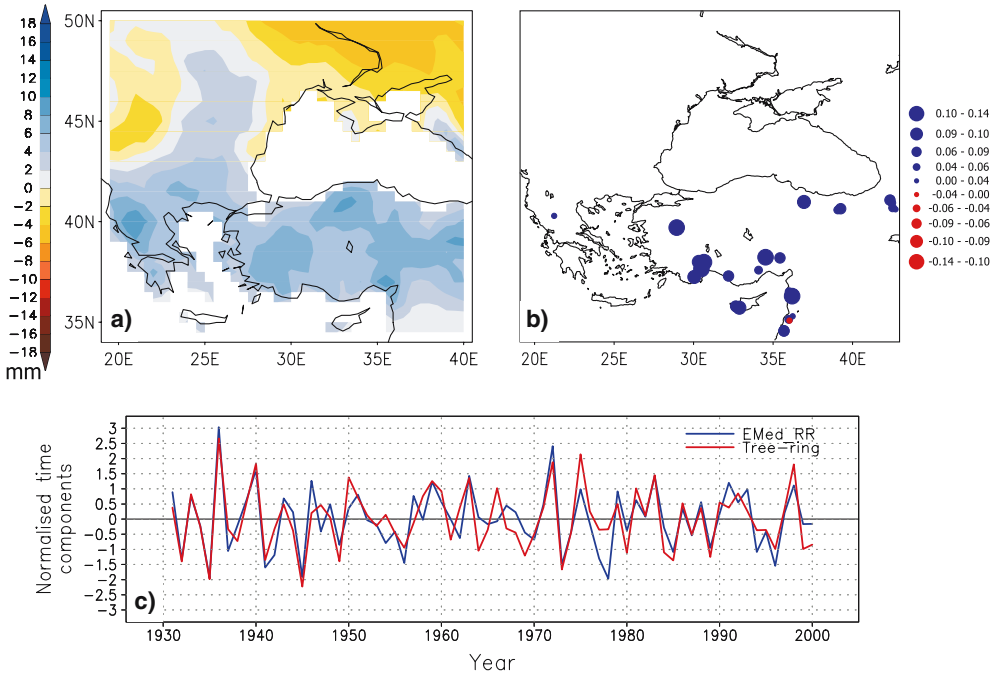

Fig. 8 Patterns of the first canonical pair of **a** May–August precipitation sum anomalies (in mm, contour interval 2 mm) and **b** tree ring width series over the 1931–2000 period. They explain 9% (precipitation) and 22% (tree-ring width) of the total variance. **c** Normalized time components of the first CCA. The correlation between the two series is 0.82

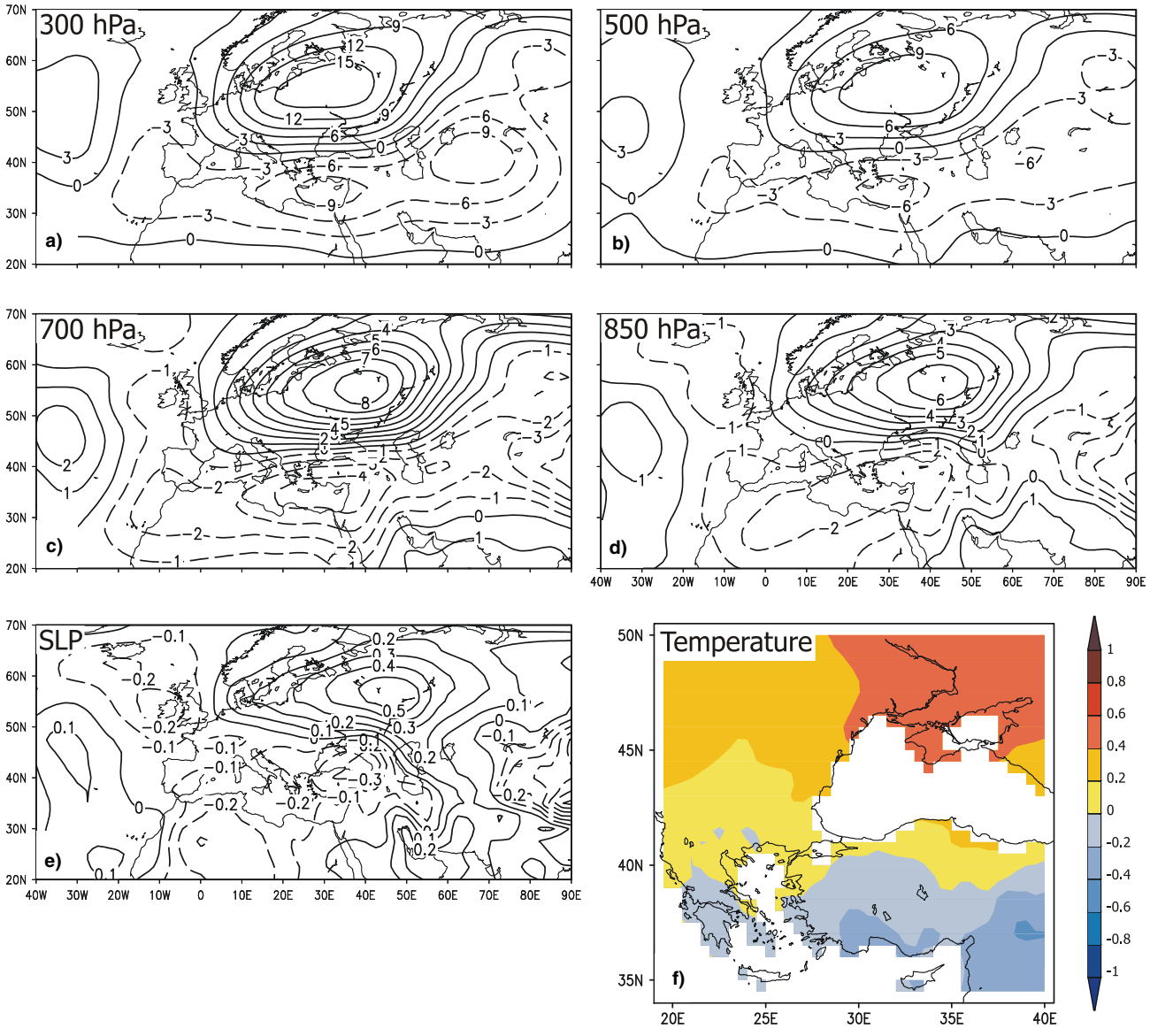

Fig. 9 Regression maps between NCEP Reanalysis large-scale variables (anomalies in gpm), gridded surface air temperature (anomalies in °C) and the first canonical series of precipitation presented in Fig. 8c over the period 1948–2000. *Solid lines* mark positive values and *dashed lines* negative values

had a duration of 5 years (1601–1605 and 1751–1755). Generally, 1, 2, and 3 year wet periods were evenly distributed throughout the reconstruction.

A May–August 5 year moving average of the precipitation reconstruction demonstrates multiannual to decadal variation and suggests several prolonged wet and dry events (Fig. 7). The driest 5-year reconstructed period was 1436–1440 (61 mm). The driest 5-year period in the instrumental data was 1941–1945 (61 mm). The wettest 5-year reconstructed period was 1751–1755 (98 mm), while the wettest period during the instrumental data was 1972–1976 (95 mm). Figure 7 shows an upward trend (though not significant) from approximately 1490–1520 followed by a period of high variability in extreme wet and dry events until the late sixteenth century. The period 1750–1780 shows a pattern of low variability. Two periods of high variability are evident from approximately 1650–1670 and from the 1850s to the 1930s. There is no significant trend detectable within the twentieth century.

5.4 Large-scale circulation patterns related to tree-ring indices AD 1931–2000

The relationship between May–August precipitation variability and the eastern Mediterranean tree-ring indices over the 1931–2000 period was studied by means of CCA in the EOF space. Canonical series and their associated spatial vectors for the leading first mode are presented in Fig. 8. These maps represent anomalies indicating realistic deviations in the physical units of

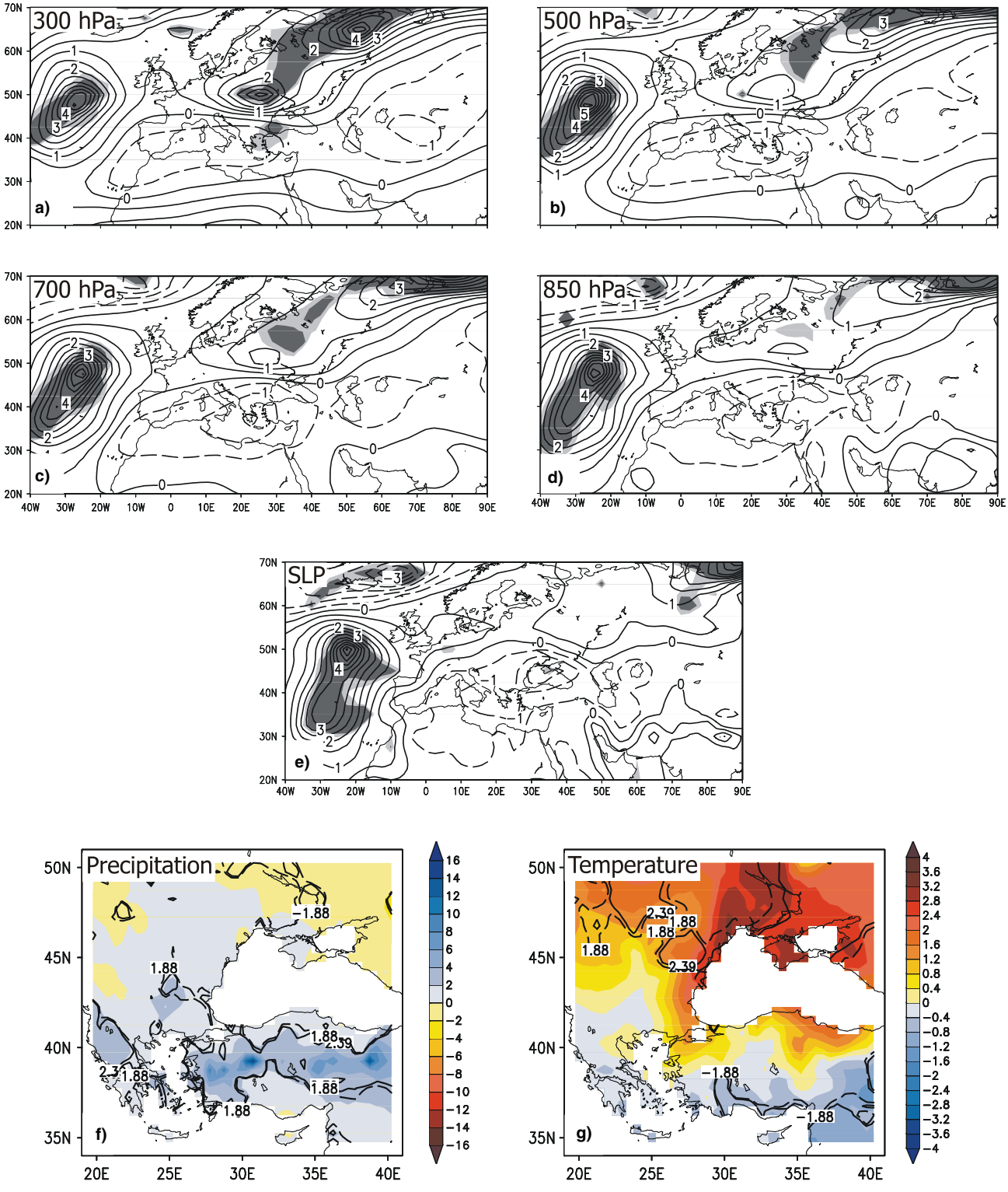

Fig. 10 Scaled anomaly composites of **a**–**d** May–August geopotential heights, **e** SLP, **f** surface air temperature and **g** precipitation anomalies for positive precipitation derived from Fig. 8c 1948–2000. Significant areas in (**a**–**e**) at the 90% and at the 95% confidence level are shaded in *light* and *dark grey* color, respectively. Significant areas in (**f**, **g**) at the 90% and the 95% are given in *dashed* and *solid* lines. Units are arbitrary. Above normal May–August precipitation characterizes the summers 1959, 1963, 1972, 1983, 1991, 1998

each variable. These figures can be interpreted with either the present sign configuration or with the opposite sign, following the sign of the time series. For both the predictor (precipitation) and the predictand (tree-ring indices), eight EOFs were retained for the subsequent CCA analysis.

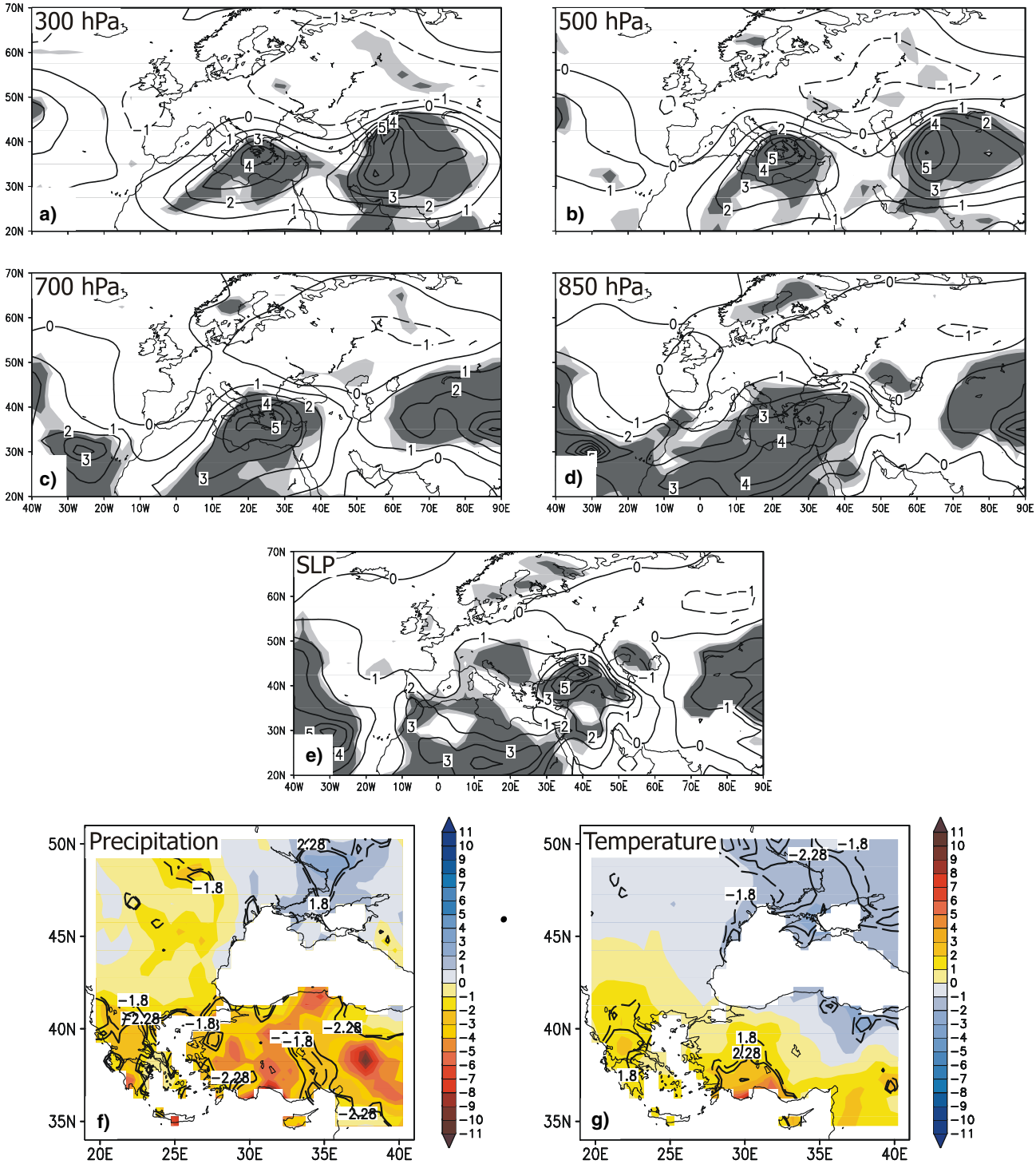

Fig. 11 Same as Fig. 10 but for the negative precipitation scores derived from Fig. 8c. Below normal May–August precipitation characterizes the years 1956, 1973, 1977, 1978, 1985, 1994, 1996

The first CCA exhibits a correlation of 0.82 between the predictor and the predictand (normalized time components; Fig. 8c). The year-to-year variation of the two time series is presented in Fig. 8c. The strong relationship between the two data sets implies that this coupled mode reflects more than half of the interaction between the tree-ring indices and May–August precipitation over the period 1931–2000. The normalized time components of the predictand and predictor represent the 'sign' corresponding to the patterns presented in Fig. 8a, b. CCA1 accounts for 22% of the total tree-ring indices for the 36 chronologies.

The canonical component of the precipitation (Fig. 8a) explains approximately 9% of the total variability. In the positive phase (positive normalized time components), the spatial pattern shows positive precipitation anomalies stretching from Greece to Turkey, to the Near East region, and parts of the Balkans. Below normal rainfall is visible north of the Black Sea. Wet conditions are associated with above normal tree-ring indices at 35 of the 36 locations. The largest anomalies occurred in the Turkish, Cypriot and Syrian series. These findings are broadly consistent with those determined using response function analysis with climate data local to the tree-ring sites (see Sect. 2.2).

Figure 9 shows the regression maps between the first canonical series of precipitation and: (1) several geopotential height variables (300, 500, 700, 850 hPa), (2) SLP as provided by the NCEP Reanalysis (Kalnay et al. 1996; Kistler et al. 2001), and (3) surface air temperature (Mitchell et al. 2004) expressed as anomalies from the 1948 to 2000 period. A CCA analysis using the 1948–2000 period revealed essentially the same results as the 1931–2000 period (not shown).

All the maps of Fig. 9 are regression maps between the resulting canonical series and the original fields. Thus, anomalies indicate realistic deviations in the physical units of each variable. The regression patterns for the geopotential height fields show a strong dipole pattern with negative anomalies south of around 40°N and positive anomalies further north connected with stronger anomalous easterlies (in absolute charts reduced westerlies, not shown) in the north. In contrast, the eastern Mediterranean region is mainly influenced by anomalous low pressure conditions and convection. These positive and negative anomalies decrease towards lower levels and disappear almost entirely at SLP. The surface air temperature regression illustrates a north-south pattern with cooler conditions south of around 40°N and above normal temperatures over the remaining areas.

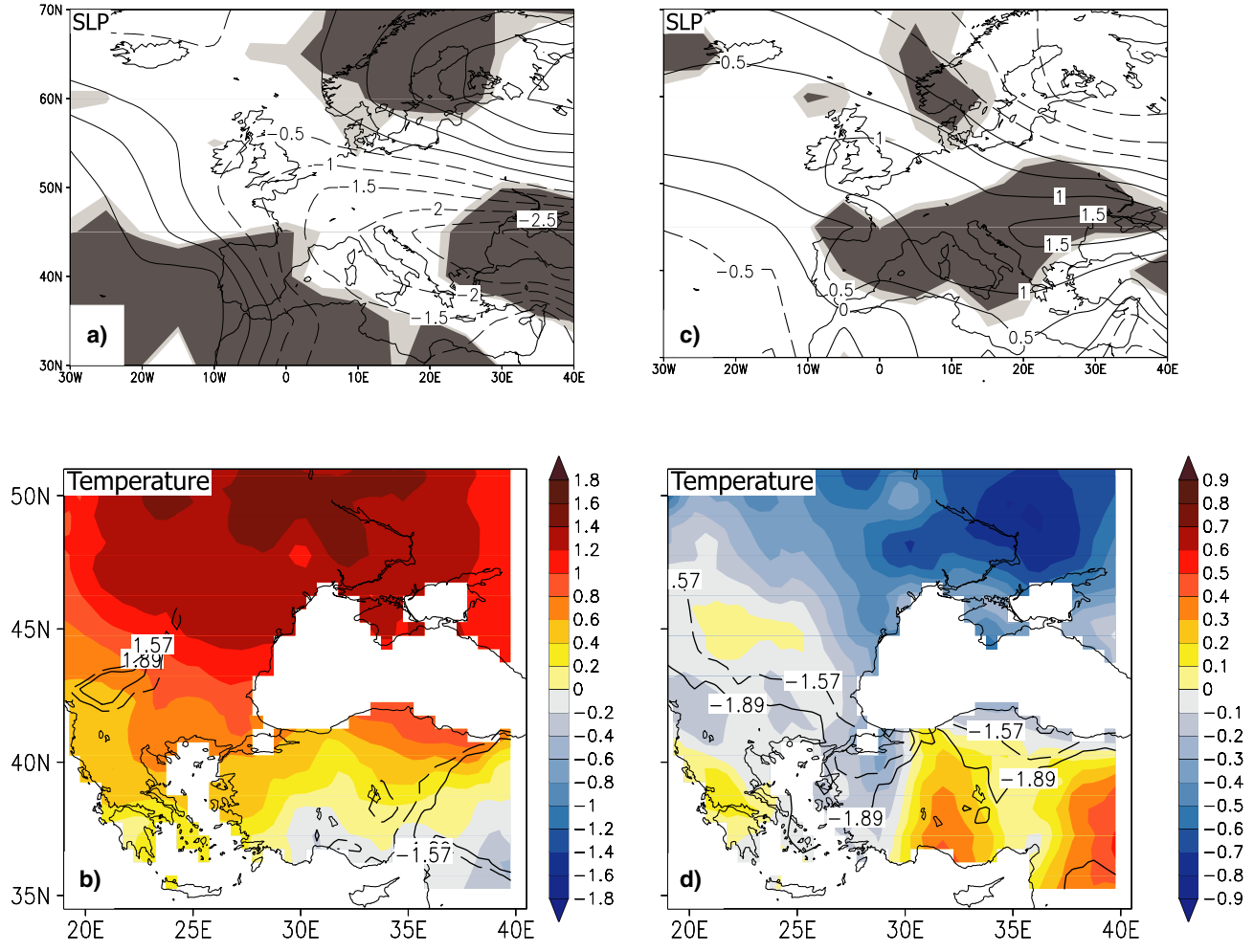

Fig. 12 Scaled anomaly composites of **a**, **c** reconstructed SLP (Luterbacher et al. 2002) **b**, **d** reconstructed temperature (Luterbacher et al. 2004) for the wettest (1.5 standard deviation; *left panel*) and driest (1.5 standard deviation; *right panel*) eastern Mediterranean summers (May–August) after 1764. Significant areas in **a**, **c** at the 90% and at the 95% confidence level are shaded in *light* and *dark grey* color, respectively. Significant areas in (**b**, **d**) at the 90% and the 95% level are given in *dashed* and *solid lines*. Units are arbitrary

In general, above (below) normal tree-ring indices over the eastern Mediterranean region in the second half of the twentieth century appear to be influenced mainly by above (below) normal May–August precipitation. This is driven by anomalous below (above) normal pressure at all levels and by convection (subsidence) and small pressure gradients at sea level. These atmospheric conditions are also responsible for the anomaly surface air temperature distribution, which indicates below (above) normal values in the southern regions and warmer (cooler) conditions north of around 40°N.

5.5 Large-scale atmospheric circulation related to tree-ring and reconstructed precipitation data

5.5.1 *Anomaly composites of high and low tree-ring width AD 1948–2000*

This section describes the spatial variability of atmospheric circulation at different levels, surface air temperature and precipitation as related to anomalous wet and dry late spring/summer seasons (derived from the first CCA time series; Fig. 8c).

Figure 10 shows the scaled anomaly (1948–2000 mean subtracted) composites of the different large-scale fields related to the precipitation scores larger than one standard deviation over the 1948–2000 period. Significance of the composite anomalies, relative to the 1948–2000 mean, was computed using 90% and 95% significance thresholds of the modified two-sided *t* test (Brown and Hall 1999).

May–August geopotential heights and SLP anomaly composites related to extreme positive precipitation over the eastern Mediterranean (Fig. 10) indicate below normal values in a zonally elongated band stretching from the southern North Atlantic to the Mediterranean, Near East, and Asia. There are only small areas within the Mediterranean that exceed the 90% and 95% significance levels of the two-sided *t* test. Above normal geopotential height and SLP values are prevalent north of around 50°N and parts of the northern North Atlantic. The anomaly composite patterns resemble the regressed patterns presented in Fig. 9 and those identified by Hughes et al. (2001) and Touchan et al. (2003).

Below-normal geopotential heights and low pressure are connected with convectivity and atmospheric instability. Low pressure systems passing over the Mediterranean (mostly in May) and other factors not directly related to the large-scale atmospheric forcing lead to significantly above-normal precipitation over the eastern Mediterranean. The lower pressure and instability are also responsible for lower temperatures over the region. High pressure and positive geopotential height anomalies in the north are significantly connected with continental dry and warm air towards the northern Black Sea region and the Balkans (Fig. 10). The same analysis

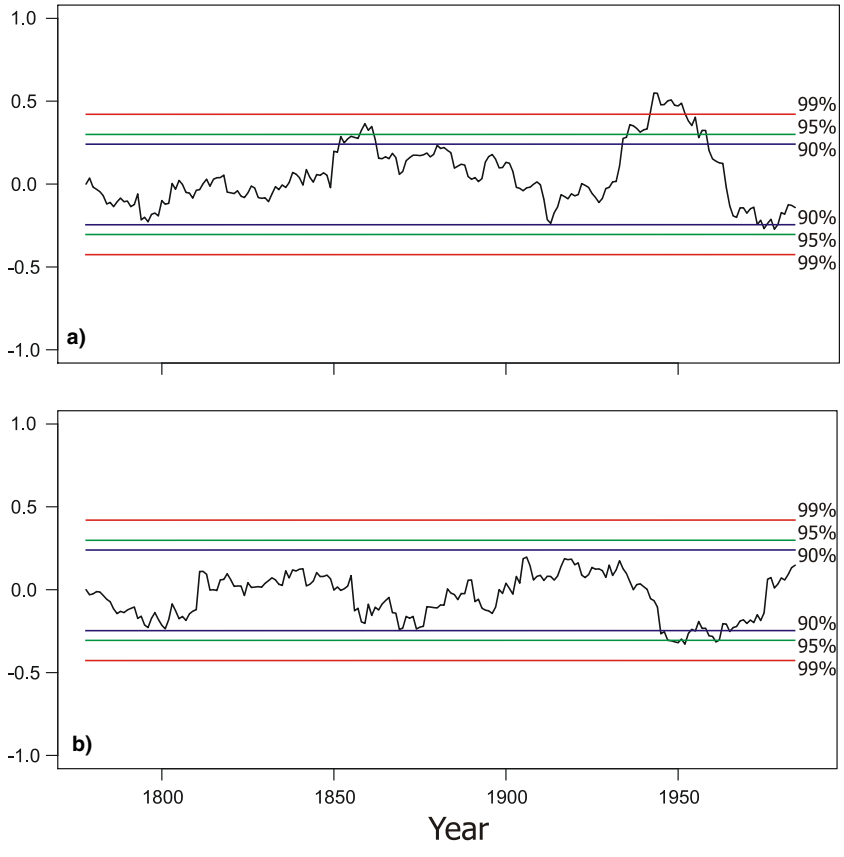

Fig. 13 Thirty year running correlation between the PCs of the first (**a**) and second (**b**) EOF of May–August SLP and May–August precipitation 1764–2000. The 90, 95 and 99% correlation significance levels have been calculated with Monte Carlo simulations

based on the ten highest tree-ring indices reveals similar results with slightly larger significant areas (not shown).

Anomaly composites related to the precipitation scores lower than one standard deviation over the period 1948–2000 are shown in Fig. 11. They resemble the reversed regression patterns shown in Fig. 9 and the dry years pattern identified by Touchan et al. (2003). The signal and significant areas are much stronger and more widespread than the anomaly composites related to positive precipitation (and thus tree-ring indices; Fig. 10). Anomalous negative precipitation (Fig. 10f) is generally connected with significantly higher geopotential height and SLP anomalies stretching from northern Africa to the eastern Mediterranean, the Caspian Seas, and Asia.

Low tree-ring indices (reduced precipitation) are thus related to a barotropic structure of the troposphere with blocking, subsidence, and stability over the eastern Mediterranean (Fig. 11a–e). This is connected with dryness and significantly higher temperatures south of around 42°N (Fig. 11f–g). Another important feature characterizing the eastern Mediterranean is a persistant inversion that prevails over the region from June to September (Dayan et al. 1988, 2002; Saaroni et al. 2003). This inversion traps lower level moisture and pollution contributing to the enhancement of heat stress over the area. The weakening of the Etesian winds, leading to a reduction in the prevailing cool advection from northwest can explain, at least in part, the significant above-normal temperatures over the eastern Mediterranean. Significantly below-normal temperatures and above normal precipitation in the north of the Black Sea can be partially explained by the anomalous weak mid to upper level trough over western Russia. This trough is associated with instability and cooler air originating in northwestern Europe.

Independent large-scale SLP and surface air temperature estimates allow us to analyze the large-scale climate patterns related to the summer precipitation extremes derived from reconstructed precipitation in an historical context. From the May–August precipitation reconstruction (Fig. 6), we selected the driest and wettest summers (exceeding 1.5 standard deviation; 16 dry and 17 wet summers) from 1764 to 2000 and calculated anomalous SLP and surface air temperature composites and their associated significant regions (Fig. 12). The driest summers from 1764 reconstructed from the tree-ring indices reveal a consistent picture with significant positive SLP anomalies over the Mediterranean similar to Fig. 11, though with shifted centers of maximum departures.

Differences in the SLP distribution and the center of largest anomalies can be related not only to uncertainties in the SLP and precipitation reconstructions for the pre-1900 period, but also to a variety of circulation patterns responsible for anomalous extremes of precipitation in the area. More important however, are the small pressure gradients during the summer and the fact that the climatic conditions are influenced mainly by regional scale processes and are more sensitive to local forcing related to insolation distribution, high sensitivity to local lower boundary conditions (soil moisture), and other effects such as topography, exposure and continentality.

There is a resemblance in terms of significant areas between the anomalous temperature patterns during the last 50 years of the twentieth century (Fig. 11) and the temperature patterns associated with dry conditions over the last 237 years (Fig. 12d). Main differences can be found over western Turkey. In general, though, our results point to the stability of the large-scale climate patterns over the last several centuries related to eastern Mediterranean extremes. They have been associated with anomalously high pressure over large parts of the Mediterranean, warmer conditions over southern and eastern Turkey as well as Near East, and cooler conditions over the western and northern Black Sea region.

Concerning the wettest summers over the eastern Mediterranean region for the 1764–2000 period (Fig. 12c), the SLP anomaly composite (Fig. 12a) shows a similar pattern compared to the wet cases over the last 50 years of the twentieth century (Fig. 10g), though with significant areas over the western and eastern Mediterranean Basin. Nevertheless, the lower pressure zone from the Atlantic through Europe to the southeastern Mediterranean points to recurrent low pressure systems bringing frontal systems from the northwest to the region. This, together with the orography and smaller scale processes that play a very significant role, leads to above normal rainfall, particularlly during late spring and summer. The anomalous temperature pattern (Fig. 12b) shows strong similarities (except for Greece) with negative values along the southern Turkish coast and the Near East region, but positive anomalies north of the Black Sea area, the Balkans and Greece.

5.5.2 *Relationship between atmospheric circulation and reconstructed precipitation from AD 1764–2000*

In addition to the analysis of wet and dry extremes in the past and present, this section examines the overall correlation and running correlations between atmospheric circulation and precipitation for the instrumental and reconstruction periods. The correlation between the first CCA precipitation scores and major teleconnection indices (http://www.cpc.ncep.noaa.gov/data/teledoc/telecontents.html; NOAA-CPC 2004) published by the NOAA Climate Prediction Center for the last 50 years indicates a significant (at the 5% level) correlation only with the East Atlantic Jet (EA-Jet) pattern. The EA-Jet is the third primary mode of low frequency variability found over the North Atlantic, appearing from April to August.

The EA-Jet pattern also shows a north-south dipole of anomaly centers, with one main center located over the high latitudes of the eastern North Atlantic and Scandinavia, and the other center located over northern Africa and the Mediterranean Sea. A positive phase of the EA-Jet pattern reflects an intensification of

westerlies over the central latitudes of the eastern North Atlantic and much of Europe (in agreement with our regression patterns, Fig. 9), while a negative phase reflects a strong split-flow configuration over these regions, sometimes in association with long-lived blocking anticyclones in the vicinity of Greenland and Great Britain (NOAA-CPC 2004). Our anomaly regression pattern at 500 hPa (Fig. 9) is similar to the first summer (JJAS) CCA results between 500 hPa and Mediterranean precipitation reported by Dünkeloh and Jacobeit (2003). They also noted a significant correlation with the EA-Jet pattern throughout the entire Mediterranean coastal area for the second part of the twentieth century.

A further investigation has been made on the strength of the correlations between the reconstructed precipitation time series and atmospheric circulation for the period 1764–2000 to see how they change over time. Thus, this analysis is an indication of potential instabilities through time and the importance of the main European atmospheric modes on regional eastern Mediterranean summer precipitation. As EA-Jet pattern reconstructions are not available prior to 1950, we performed running correlations for overlapping 30-year periods between the first and second principal components of the North Atlantic/European SLP and reconstructed precipitation (Fig. 13). The significance of the correlation coefficients is based on the calculation of 1,000 Monte Carlo simulations.

The first EOF of May–August SLP for the period 1764–2000 explains 32% of the total May–August SLP variability and reveals a monopole pattern with negative anomalies centered over the British Isles (not shown). The Mediterranean area is at the southern border of this negative anomaly pattern. This pattern strongly resembles the EA-Jet anomaly pattern described above. Interestingly, the first SLP PC correlates significantly at the 99% level ($r = 0.35$) with the EA-Jet index over the common period 1950–2000. Thus, this PC can be considered a 'proxy' for the EA-Jet over the last 237 years.

The second EOF accounts for 23.3% of summer SLP variance and is connected with positive pressure anomalies south of approximately 55°N and below normal SLP centered over Iceland (not shown). As expected, the correlations between the main modes of summer atmospheric circulation and eastern Mediterranean precipitation are weak and often statistically insignificant. For the first PC, significant positive correlations are found shortly after 1850 and during the middle of the twentieth century, but with negative correlations over the last few decades (Fig. 13a). These analyses suggest that recent significant correlation with the EA-Jet pattern is not stable through time. We believe that changing climatic conditions are responsible for this apparent disagreement. The 30 year-running correlation between the second SLP EOF and precipitation reveals mostly insignificant relationships, except for the middle of the twentieth century (Fig. 13b).

Similar findings on non-stationary relations between atmospheric circulation and European climate covering the past few centuries have been found recently (e.g. Schmutz et al. 2000; Jacobeit et al. 2001, 2003; Slonosky et al. 2001; Slonosky and Yiou 2002; Jones et al. 2003; Timm et al. 2004). Jacobeit et al. (2003) report that during July, the long-term evolution of increasing anticyclonicity over Europe has strengthened during the last 50 years, becoming recently a unique phenomenon within the last centuries and causing an unprecedented decline in Central European July precipitation during the second half of the twentieth century.

We did not find a reduction of precipitation over the same period for southeastern Europe. However, July precipitation over this area is almost exclusively connected to smaller scale processes and local factors. Further, climate variations of the atmospheric circulation, or changes in the probability distribution of circulation modes induced by anthropogenic effects, are likely to project onto the natural modes during the twentieth century (e.g. Hsu and Zwiers 2001). From this fact one would conclude that EA-Jet or any other teleconnection index reconstructions based on the eastern Mediterranean precipitation (or tree-ring information) data for the second half of the twentieth century would be less representative than in pre-industrial times.

6 Conclusions

This study represents the first large-scale systematic dendroclimatic sampling focused on developing chronologies from Turkey, Syria, Lebanon, Cyprus, and Greece. It demonstrates that annual tree-ring growth from the region contains excellent records of May–August precipitation. Extending annual observed climatic data through dendrochronology offers new perspectives on the level, variability, and duration of past climatic trends and extreme events. The reconstruction of late spring/summer (May–August) precipitation also provides a climate variable with annual resolution that adds a new dimension to the environmental contexts historians and archaeologists working in the region can use for their descriptions and interpretations of human social and population dynamics.

Multiannual and decadal variations are evident in the May–August precipitation reconstruction. There is an upward, though not significant, trend from approximately 1490–1520 followed by high variation in extreme wet and dry events until the late sixteenth century. Two periods of high variability are evident from approximately 1650–1670 and from the 1850s to the 1930s. There is no significant trend detectable in the twentieth century. The longest dry period during the past six centuries lasted 5 years (1591–1595) and occurred only once during the last 600 years. The longest wet period during the past 600 years also lasted 5 years (1601–1605 and 1751–1755).

We found that tree-ring indices in the area are sensitive mainly to May–August precipitation and, to a lesser extent, temperature. Strong (weak) tree-ring growth is associated with above (below) normal precipitation over large parts of eastern Mediterranean. Above (below) normal precipitation in these areas can be related to anomalous below (above) normal SLP over the larger Mediterranean area, connected with convective instability (stability). A novel comparison with independent reconstructions of surface air temperature and SLP since 1764 suggests that similar main climate modes over the recent 50 years and the last 237 years are related to anomalous wet and dry summers. Running correlation series calculated over 30-year windows reveal non-stationarities and mostly insignificant relationships between atmospheric circulation and eastern Mediteranean summer precipitation and also, tree-ring indices on decadal time scales, suggesting caution must be used in extrapolating current relationships between circulation and tree-ring indices. In addition to atmospheric influence on regional tree-ring data, other processes such as convective instability, land-sea interactions, orography, and thermally induced local precipitation events are also relevant.

Acknowledgments The authors wish to thank the Ministry of Forestry, Southwest Anatolia Forest Research Institute (SAFRI), the Director Mr. Yusuf Cengiz for his great help and support in making this study possible. We would like also to thank the Lebanon Ministry of Agriculture, Department of Forestry, the Director Mr. Ghattas Ak and Assistant Director Mr. Fadi Asmer; the University of Aleppo, Faculty of Agriculture; the Cyprus Ministry of Agriculture, Department of Forestry and the Cyprus Forestry College, Cyprus Meteorological Service, Dr. Andreas Christou, Mr. Christos Alexandrou, and Mr. Stelios Pashiardis; and University of Patras, Botanical Institute, Department of Biology, Greece, Mr. Dimitris Sarris and Dr. Dimitris Christodoulakis for their help and support. We thank Drs. Peter Kuniholm and Maryanne Newton, Malcolm and Carolyn Wiener Laboratory for Aegean and Near Eastern Dendrochronology, Cornel University for their assistance and for providing us with some of their *C. libani* samples from Lebanon. We thank Drs. Gregg Garfin, Dave Meko, and Martin Munro for their advice and suggestions. We thank Brian Wallen, Maher Qishawi, Necati Bas, Erdogan Uzun, Nşsibe Dağdeviren Galip Yanik, and Evan Adams for their valuable assistance in the field; we thank Melissa Hubbard, Christopher Shuler, Chandler Birch, and Candice Marburger for their assistance in sample preparation and measurement. We thank Mr. Richard Warren for his independent verification of our cross-dating of some of the samples. We thank Dr. J. Fidel Gonzar Rouco and Mr. Paul Della-Marta for statistical advice. We thank Dr. Murat Türkes for providing his climate classification scheme from Turkey. We thank the Tyndall Center for allowing us to use the Mitchell et al. (2004) temperature and precipitation data. We wish to thank the anonymous reviewers for their constructive comments and suggests on the manuscript. Funding was provided by the US National Science Foundation, Earth System History (Grant No. 0075956). Elena Xoplaki was partially supported by Fifth Framework Programme of the European Union (project SOAP), the Swiss Science Foundation (NCCR Climate) and US National Science Foundation, Earth System History (Grant No. 0075956). Jürg Luterbacher was supported by the Swiss Science Foundation (NCCR Climate). Finally, we thank our close friend, the late Richard Holmes for his great support and advice since the inception of this project.

References

Akkemik Ü, Aras A (2005) Reconstruction (A.D. 1689–1994) of April–August precipitation in southern part of central Turkey. Int J Climatol (in press)

Akkemik Ü, Dağdeviren N, Aras A (2005) A preliminary reconstruction (A.D. 1635–2000) of spring precipitation using oak tree rings in the western Black Sea region of Turkey. Int J Biomet. DOI 10.1007/s00484-004-0249-8

Akkemik Ü (2000) Dendroclimatology of umbrella pine (*Pinus pinea* L.) in Istanbul, Turkey. Tree Ring Bull 56:17–23

Alpert P, Abramski R, Neeman BU (1990) The prevailing summer synoptic system in Israel—subtropical high, not Persian trough. Isr J of Earth Sci 39:93–102

Baisan CH, Swetnam TW (1990) Fire history on a desert mountain range: Rincon Mountain Wilderness, Arizona, USA. Can J Forest Res 20:1559–1569

Barnett TP, Preisendorfer RW (1987) Origins and levels of monthly and seasonal forecast skill for United States air temperature determined by canonical correlation analysis. Mon Wea Rev 115:1825–1850

Bartzokas A, Lolis CJ, Metaxas DA (2003) The 850 hPa relative vorticity centres of action for winter precipitation in the Greek area. Int J Climatol 23:813–828

Bitan A, Saaroni H (1992) The horizontal and vertical extension of the Persian Gulf trough. Int J Climatol 12:733–747

Briffa KR, Jones PD, Schweingruber FH, Karlén W, Shiyatov SG (1996) Tree-ring variables as proxy-indicators: problems with low-frequency signals. In: Jones PD, Bradley RS, Jouzel J (eds) Climatic variations and forcing mechanisms of the last 2000 years. NATO ASI Series I41, pp 9–41

Briffa KR, Osborn TJ, Schweingruber FH (2004) Large-scale temperature inferences from tree rings: a review. Global Planet Change 40:11–26

Brown TJ, Hall BL (1999) The use of t values in climatological composite analyses. J Clim 1:2941–2945

Chbouki N (1992) Spatio-temporal characteristics of drought as inferred from tree-ring data in Morocco. PhD dissertation, The University of Arizona, Tucson

Cook ER (1985) A time-series analysis approach to tree-ring standardization. PhD Dissertation, Department of Geosciences, The University of Arizona, Tucson

Cook ER, Briffa KR (1990) A comparison of some tree-ring standardization methods. In: Cook ER, Kairiukstis LA (eds) Methods of dendrochronology. Kluwer, Dordrecht, pp 104–123

Cook ER, Briffa KR, Jones PD (1994) Spatial regression methods in dendroclimatology—a review and comparison of two techniques. Int J Climatol 14:379–402

Corte-Real J, Zhang X, Wang X (1995) Large-scale circulation regimes and surface climatic anomalies over the Mediterranean. Int J Climatol 15:1135–1150

Cullen HM, deMenocal PD (2000) North Atlantic influence on Tigris-Euphrates streamflow. Int J Climatol 20:853–863

Cullen HM, Kaplan A, Arkin PA, deMenocal PD (2002) Impact of the North Atlantic Oscillation on middle eastern climate and streamflow. Clim Change 55:315–338

Dünkeloh A, Jacobeit J (2003) Circulation dynamics of Mediterranean precipitation variability 1948–1998. Int J Climatol 23:1843–1866

D'Arrigo R, Cullen H (2001) A 350-yr reconstruction of Turkish precipitation. Dendrochronologia 19:169–177

Dayan U, Shenhav R, Graber M (1988) The spatial and temporal behavior of the mixed layer in Israel. J Appl Meteorol 27:1382–1394

Dayan U, Lifshitz-Goldreich B, Pick K (2002) Spatial and structural variation of the atmospheric boundary layer during summer in Israel-Profiler and rawinsonde measurements. J Appl Meteorol 41:447–457

Dracup JA, Lee KS, Paulson EG Jr (1980) On the definition of droughts. Water Resour Res 16:297–302
Edwards AL (1984) An introduction to linear regression and correlation, 2nd edn. WH Freeman, New York, pp 81–83
Eshel G, Farrell BF (2000) Mechanisms of Eastern Mediterranean rainfall variability. J Atmos Sci 57:3219–3232
Eshel G, Cane MA, Farrell BF (2000) Forecasting Eastern Mediterranean drought. Mon Weather Rev 128:3618–3630
Esper J, Frank DC, Wilson JS (2004) Climate reconstructions: low-frequency ambition and high-frequency ratification. Eos 85:113–120
Fernández J, Saenz J, Zorita E (2003) Analysis of wintertime atmospheric moisture transport and its variability over Southern Europe in the NCEP-reanalyses. Clim Res 23:195–215
Fritts HC (1976) Tree Rings and climate. Academic Press, New York
Fritts HC (1991) Reconstructing large-scale climatic patterns from tree-ring data: A diagnostic analysis. The University of Arizona Press, Tucson
Fritts HC, Guiot J (1990) Methods of calibration, verification and reconstruction. In: Cook ER, Kairiukstis LA (eds) Methods of dendrochronology: applications in the environmental sciences, International institute for applied systems analysis. Kluwer, Boston, pp 163–176
Fritts HC, Shashkin AV (1995) Modeling tree-ring structure as related to temperature, precipitation, and day length. In: Lewis TE (ed) Tree rings as indicators of ecosystem health. CRC Press, Ann Arbor Michigan, pp 17–57
Fritts HC, Guiot J, Gordon G (1990) Verification. In: Cook ER, Kairiukstis LA (eds) Methods of dendrochronology: applications in the environmental sciences, International institute for applied systems analysis. Kluwer, Boston, pp 178–184
Gassner G, Christiansen-Weniger F (1942) Dendroklimatologische Untersuchungen über die Jahresringentwicklung der Kiefern in Anatolien. Nova Acta Leopoldina: Abhandlung der Kaiserlich Leopoldinisch-Carolinisch deutschen Akademie der Naturforscher NF, Band 12, Nr 80
Gershunov A, Schneider N, Barnett T (2001) Low-frequency modulation of the ENSO–Indian monsoon rainfall relationship: signal or noise? J Clim 14:2486–2492
Hsu CJ, Zwiers FW (2001) Climate change in recurrent regimes and modes of Northern Hemisphere atmospheric variability. J Geophys Res 106:20145–20159
Hughes MK (2002) Dendrochronology in climatology—the state of the art. Dendrochronologia 20:95–116
Hughes MK, Vaganov EA, Shiyatov SA, Touchan R, Funkhouser G (1999) Twentieth-century summer warmth in northern Yakutia in a 600-year context. Holocene 9:603–608
Hughes MK, Kuniholm PI, Eischeid JK, Garfin G, Griggs CB, Latini C (2001) Aegean tree-ring signature years explained. Tree Ring Res 57:67–73
Hurrell JW (1996) Influence of variations in extratropical wintertime teleconnections on Northern Hemisphere temperature. Geophys Res Lett 23:665–668
Jacobeit J, Jönsson P, Bärring L, Beck C, Ekström M (2001) Zonal indices for Europe 1780–1995 and running correlation with temperature. Clim Change 48:219–241
Jacobeit J, Wanner H, Luterbacher J, Beck C, Philipp A, Sturm K (2003) Atmospheric circulation variability in the North-Atlantic-European area since the mid-seventeenth century. Clim Dyn 20:341–352. DOI 10.1007/s00382-002-0278-0
Jones PD, Mann ME (2004) Climate over past millennia. Rev Geophys 42:RG2002. DOI 10.1029/2003RG000143
Jones PD, Briffa KR, Barnett T, Tett S (1998) High resolution paleoclimatic records for the last millennium: interpretation, integration and comparison with General Circulation Model control-run temperature. Holocene 8:455–471
Jones PD, Osborn TJ, Briffa KR (2003) Pressure-based measures of the North Atlantic Oscillation (NAO): a comparison and an assessment of changes in the strength of the NAO and in its influence on surface climate parameters. In: Hurrell JW, Kushnir Y, Ottersen G, Visbeck M (eds) The North Atlantic Oscillation: climatic signifcance and environmental impact. Geophysical Monograph 134, American Geophysical Union, Washington, pp 51–62
Kalnay E et al. (1996) The NCEP/NCAR 40-year reanalysis project. Bull Am Meteorol Soc 77:437–471
Kistler R et al. (2001) The NCEP-NCAR 50-year reanalysis: monthly means CD-ROM and documentation. Bull Am Meteorol Soc 82:247–267
Kuniholm PI (1990) The archaeological record: evidence and non-evidence for climate change. In: Runcorn SJ, Pecker J-C (eds) The Earth's climate and variability of the sun over recent millennia. Phil Trans R Soc Lond A, pp 645–655
Lolis CJ, Bartzokas A, Metaxas DA (1999) Spatial covariability of the climatic parameters in the Greek area. Int J Climatol 19:185–196
Livezey RE, Smith TM (1999) Considerations for use of the Barnett and Preisendorfer (1987) algorithm for canonical correlation analysis of climate variations. J Climate 12:303–305
Luterbacher J, Xoplaki E, Dietrich D, Rickli R, Jacobeit J, Beck C, Gyalistras D, Schmutz C, Wanner H (2002) Reconstruction of sea level pressure fields over the eastern North Atlantic and Europe back to 1500. Clim Dyn 18:545–561. DOI 10.1007/s00382-001-0196-6
Luterbacher J, Dietrich D, Xoplaki E, Grosjean M, Wanner H (2004) European seasonal and annual temperature variability, trends, and extremes since 1500. Science 303:1499–1503. DOI 10.1126/science.1093877
Mann ME (2002) Large-scale climate variability and connections with the Middle East in past centuries. Clim Change 55:287–314
Meko DM (1997) Dendroclimatic reconstruction with time varying subsets of tree indices. J Climate 10:687–696
Meko DM, Graybill DA (1995) Tree-ring reconstruction of Upper Gila River Discharge. Water Resour Bull 31:605–616
Meko DM, Therrell MD, Baisan CH, Hughes MK (2001) Sacramento river flow reconstructed to A.D. 869 from tree rings. Am Water Resour Assoc 37(4):1020–1037
Mitchell TD, Carter TR, Jones PD, Hulme M, New M (2004) A comprehensive set of high-resolution grids of monthly climate for Europe and the globe: the observed record (1901–2000) and 16 scenarios (2001–2100). Tyndall Centre Working Paper 55
NOAA-CPC (2004) Northern Hemisphere teleconnection indices (1950–2004; monthly). http://www.cpc.ncep.noaa.gov/data/teledoc/telecontents.html
North GR, Bell TL, Cahalan RF, Moeng FJ (1982) Sampling errors in the estimation of empirical orthogonal functions. Mon Wea Rev 110:699–706
Purgstall BJVH (1983) Ottoman state history, vol 1–7. Translator: Vecdi Bürün, Üçdal Publishing, Istanbul (in Turkish)
Quadrelli R, Pavan V, Molteni F (2001) Wintertime variability of Mediterranean precipitation and its links with large-scale circulation anomalies. Clim Dyn 17:457–466
Saaroni H, Ziv B, Edelson J, Alpert P (2003) Long-term variations in summer temperatures over the Eastern Mediterranean. Geophys Res Lett 30:1946 DOI 10.1029/2003GL017742
Schmutz C, Luterbacher J, Gyalistras D, Xoplaki E, Wanner H (2000) Can we trust proxy-based NAO index reconstructions? Geophys Res Lett 27:1135–1138
Shindell DT, Miller RL, Schmidt GA, Pandolfo L (1999) Simulation of recent northern winter climate trends by greenhouse-gas forcing. Nature 399:452–455
Slonosky VC, Yiou P (2002) Does the NAO index represent zonal flow? The influence of the NAO on North Atlantic surface temperature. Clim Dyn 19:17–30
Slonosky VC, Jones PD, Davies TD (2001) Atmospheric circulation and surface temperature in Europe from the 18th century to 1995. Int J Climatol 21:63–75
Snee RD (1997) Validation of regression models: methods and examples. Technometrics 19:415–428
Stokes MA, Smiley TL (1996) An introduction to tree-ring dating. The University of Arizona Press, Tucson
von Storch H, Zwiers FW (1999) Statistical analysis in climate research. Cambridge University Press, UK

Swetnam TW (1985) Using dendrochronology to measure radial growth of defoliated trees. USDA Forest Service, Cooperative State Research Service. Agriculture Handbook No. 639, 1–39

Swetnam TW (1993) Fire history and climate change in giant sequoia groves. Science 262:885–889

Tarawneh Q, Kadioglu M (2003) An analysis of precipitation climatology in Jordan. Theor Appl Climatol 74:123–136

Thompson DWJ, Wallace JM (1998) The Arctic Oscillation signature in the wintertime geopotential height and temperature fields. Geophys Res Lett 25:1297–1300

Timm O, Ruprecht E, Kleppek S (2004) Scale-dependent reconstruction of the NAO index. J Clim 17:2157–2169

Touchan R, Hughes MK (1999) Dendrochronology in Jordan. J Arid Environ 42:291–303

Touchan R, Allen C, Swetnam TW (1996) Fire history and climatic patterns in ponderosa pine and mixed-conifer forests of the Jemez Mountains, Northern New Mexico. In: Proc Symposium on La Mesa Fire. USDA Forest Service, Rocky Mountain Forest and Range Experiment Station General Technical Report, vol 286, pp 33–46

Touchan R, Meko DM, Hughes MK (1999) A 396-year reconstruction of precipitation in Southern Jordan. J Am Water Resour Assoc 35:45–55

Touchan R, Garfin GM, Meko DM, Funkhouser G, Erkan N, Hughes MK, Wallin BS (2003) Preliminary reconstructions of spring precipitation in southwestern Turkey from tree-ring width. Int J Climatol 23:157–171

Touchan R, Funkhouser G, Hughes MK, Erkan N (2004) Standardized precipitation indices reconstructed from tree-ring width for the Turkish region. Clim Change (in press)

Tsiourtis NX (2001) Drought management plans for the Mediterranean region. Report of the Water Development Department, Nicosia, Cyprus. http://www.pio.gov. cy/wdd/eng/scientific_articles/archieve2001/article03.htm

Türkeş M (1996) Spatial and temporal analysis of annual rainfall variations in Turkey. Int J Climatol 16:1057–1076

Türkeş M (1998) Influence of geopotential heights, cyclone frequency and southern oscillation on rainfall variations in Turkey. Int J Climatol 18:649–680

Türkeş M, Erlat E (2003) Precipitation changes and variability in Turkey linked to the North Atlantic Oscillation during the period 1930–2000. Int J Climatol 23:1771–1796

Türkeş M, Erlat E (2005) Climatological responses of winter precipitation in Turkey to variability of the North Atlantic Oscillation during the period 1930–2001. Theor Appl Climatol. DOI:10.1007/s00704-004-0084-1

Türkeş M, Sümer UM, Kılıç G (2002) Persistence and periodicity in the precipitation series of Turkey and associations with 500 hPa geopotential heights. Clim Res 21:59–81

Weisberg R (1985) Applied linear regression. Wiley, New York

Widmann M (2004) One-dimensional CCA and SVD and their relationship to regression maps. J Clim (in press)

Wigley TML, Briffa KR, Jones PD (1984) On the average value of correlated time series with applications in dendroclimatology and hydrometeorology. J Clim Appl Meteorol 23:201–213

Wilks DS (1995) Statistical methods in the atmospheric sciences: an introduction. International Geophysics Series, vol 59. Academic Press, New York

Xoplaki E, González-Rouco JF, Gyalistras D, Luterbacher J, Rickli R, Wanner H (2003a) Interannual summer air temperature variability over Greece and its connection to the large-scale atmospheric circulation and Mediterranean SSTs 1950–1999. Clim Dyn 20:537–554. DOI 10.1007/s00382-002-0291-3

Xoplaki E, Luterbacher J, Burkard R, Patrikas I, Maheras P (2000) Connection between the large-scale 500 hPa geopotential height fields and precipitation over Greece during wintertime. Clim Res 14:129–146

Xoplaki E, González-Rouco JF, Luterbacher J, Wanner H (2003b) Mediterranean summer air temperature variability and its connection to the large-scale atmospheric circulation and SSTs. Clim Dyn 20:723–739. DOI 10.1007/s00382-003-0304-x

Xoplaki E, González-Rouco JF, Luterbacher J, Wanner H (2004) Wet season Mediterranean precipitation variability: influence of large-scale dynamics and trends. Clim Dyn 23:63–78. DOI 10.1007/s00382-004-0422-0

Ziv B, Saaroni H, Alpert P (2004) The factors governing the summer regime of the eastern Mediterranean. Int J Climatol 24:1859–1871

Ziv B, Saaroni H, Baharad A, Yekutieli D, Alpert P (2005) Indications for aggravation in summer heat conditions over the Mediterranean basin. Geophys Res Lett (in press)

Zorita E, Kharin V, von Storch H (1992) The atmospheric circulation and sea surface temperature in the North Atlantic area in winter: their interaction and relevance for Iberian precipitation. J Clim 5:1097–1108